WATER AND BIOLOGICAL MACROMOLECULES

FRANCESCO MALLAMACE,[1,2] CARMELO CORSARO,[1]
DOMENICO MALLAMACE,[3] H. EUGENE STANLEY,[4]
and SOW-HSIN CHEN[2]

[1]*Dipartimento di Fisica and CNISM, Università di Messina, I-98166 Messina, Italy*
[2]*Department of Nuclear Science and Engineering, Massachusetts Institute of Technology, Cambridge, MA 02139, USA*
[3]*Dipartimento di Scienze degli Alimenti e dell' Ambiente, Università di Messina, I-98166 Messina, Italy*
[4]*William Fairfield Warren Distinguished Professor; Professor of Physics; Professor of Chemistry; Professor of Biomedical Engineering; Professor of Physiology, Center for Polymer Studies, Department of Physics, Boston University, Boston, MA 02215, USA*

CONTENTS

Liquid Polymorphism: Advances in Chemical Physics, Volume 152, First Edition.
Edited by H. Eugene Stanley.

I. INTRODUCTION

From ancient times, understanding the role of water in its many aspects has been a perennial quest in both philosophy and science. Four millennia ago, Homer in the Iliad (Iliad XIV vv 201 and 244) described water as an "ocean," a big river that circumscribes and encircles the "fecund earth," and "[that] from which all the gods proceed." In his First Book on *Metaphysics* (Metaph. A 3, 983 b 6 sgg.), Aristotle initiated Western philosophy's search for the "principle element" of all things, an element out of which all other things would be generated and into which they would be resolved at their end. Through it all, the element itself would be unchanged. Thales of Miletus (VIth century BCE), the father of geometry and first philosopher of Western history, also sought this principle element and came to the conclusion that it was indeed water. Both Aristotle and Theophrastus in response to the Thales speculation and based on their own empirical observations concurred that water was the "principle" of biology and thus of all living things.

Our focus is on biological water, that is, water located in living systems. In biology, water may be located on surfaces, in little cavities or bilayers, inside macromolecules, vesicles, or near specific chemical groups. Water–amphiphile systems are one example of complex water in biology. Amphiphilic molecules are approximately linear molecules characterized by a hydrophilic head and hydrophobic terminal groups that organize into biological membranes. When water is mixed with these systems, the competition between hydrophilicity and hydrophobicity causes an entropy decrease that gives rise to the buildup of structures that, depending on variables such as temperature and concentration, assume different geometric forms (spheres, ellipsoids, cylinders, layers, and bilayers). Hydrophobicity and hydrophilicity have different effects on the local structure of water—hydrophilicity enhances it and hydrophobicity weakens it. It, thus, seems clear that the complexity of physico-chemical phenomena is due to water when it hydrates a biological structure, for example, in proteins there are many hydrophilic and hydrophobic groups distributed with some specific order inside the macromolecule. This suggests at least two questions: (i) If biological water is a form of confined water, does the physics of biological water differ from that of bulk water? (ii) Does water drive the properties of a biological system or do those properties function independently of water? We will attempt to answer these two questions.

The role that water plays in controlling the structure and dynamics of biopolymers is a fascinating research subject. While water has been considered "life's solvent" (i.e., a uniform background) for a long time, only recently it has became an active constituent of cell biochemistry [1]. A striking example of the importance of water in biosystems is that without water a protein cannot function, but a single layer of water surrounding it (called the first hydration layer) restores biological activity [2–4]. Hydration is a process. Adding water incrementally to a dry protein eventually reaches a hydration level beyond which further addition of water

no longer changes the protein properties but only dilutes them [2]. The hydration shell is thus a monolayer that covers the protein surface. Water outside this monolayer is perturbed to a smaller extent that is typically not detectable experimentally (e.g., by measuring heat capacity). The study of the reaction of lysozyme with the hexasaccharide of *N*-acetylglucosamine over the full hydration range has yielded a threshold hydration level of $h = 0.2$ [3], where h is the ratio in grams between water and dry protein. Reference [3] clearly shows that enzymatic activity closely parallels the development of surface motion and is thus responsible for protein functionality.

Understanding the relationship between the properties of proteins [4] and their associated water [5–7] is an ongoing challenge. Many biological functions [3] can be understood only if we know the structure and function of the first hydration layer. When a protein is in solution, there are two categories of water molecule in close proximity to it, (i) internal bound molecules and (ii) hydration water molecules. The internal bound molecules, located in cavities of the protein, play a structural role in protein folding.

At low T, a protein exists in a state [8,9] without conformational flexibility. As T increases, the atomic motional amplitude initially increases linearly, as in a harmonic solid. In hydrated proteins, at $T \sim 220$K, the rate of amplitude suddenly increases with T, signaling the onset of a more liquid-like motion [10–12]. This *dynamic transition* is a *protein glass transition* triggered by the coupling of the protein with the hydration water through hydrogen bonding (HB), since hydration water shows a dynamic transition at a similar temperature [12]. Whereas the process governing biological properties of proteins occurs at high T, just below the onset of protein denaturation. A protein is in the native state up to a given T^* and evolves, on increasing T, into a region characterized by a reversible unfolding–folding process. Depending on the chemical nature of the protein and the solvent, in the case of the water–lysozyme system this unfolding–folding process occurs in the range $310\text{K} < \text{T} < 360\text{K}$. Above 355K, lysozyme denatures irreversibly and calorimetric measurements [13,14] show a broad peak in the specific heat around that temperature ($T = 346$K). All the observed data confirm that the first step of denaturation of a small globular protein like lysozyme is a reversible conformational (unfolding) transition, and that the second step is irreversible. Hence, the dramatic change in the protein structure is driven by the HBs between the protein and its hydration water. The process rate constant varies with T according to an Arrhenius law, with an activation energy typical of the strength of the HB [14]. Assuming that the HB structure is closely related to the proton chemical shift δ (PCS), we use NMR to measure the configurational specific heat of water $C_{P,\text{conf}}(T)$. Figure 1 shows the $C_P(T)$ results of the hydrated protein lysozyme with an hydration factor $h = 0.3$. This data is obtained by means of a more conventional experiment on the same protein with $h = 8.3$ [14], and it illustrates well the case in which there are two crossovers [15]. Using a double scale plot, the left-hand side of Fig. 1 shows

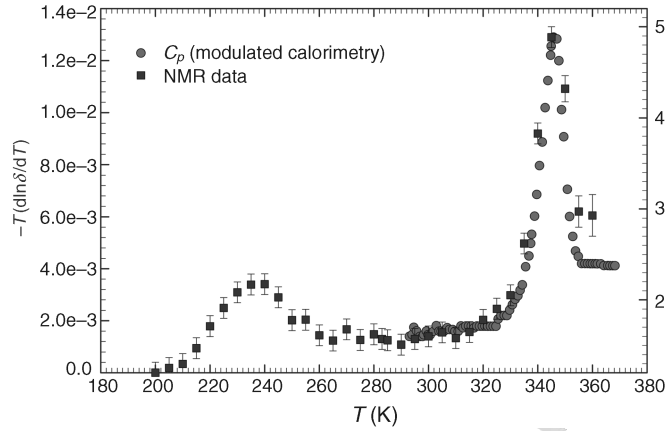

Figure 1. A comparison between the conformational heat capacity obtained from NMR [15] and calorimetric C_P data in the water–lysozyme system [14].

the configurational heat capacity, $C_{P,\mathrm{conf}}(T) \propto -T(\partial \ln \delta(T)/\partial T)_P$ for lysozyme hydration water, and the right-hand side of Fig. 1 shows $C_P(T)$ measured in the T region of the reversible unfolding–folding process. Note that $-T(\partial \ln \delta(T)/\partial T)$ displays two maxima, the first on crossing the Widom line $T_W(P)$ as proposed by different studies on hydrated proteins [16,17], and the second at a T nearly coincident with the protein denaturation process. The first maximum, at about 235K, that is, the same temperature of that of confined water, is proof that both are due to the same structural change of water. In fact, at T_W the low-density liquid (LDL) phase dominates the water properties [18,19].

On the basis of these considerations, we report here the results obtained by experiments and MD simulations on the dynamics of hydration water in biomolecules (lysozyme, DNA, and ribonucleic acid (RNA)). The findings explain how hydration water drives biomolecule activity. Specifically, we report the experimental results of light (FTIR) and neutron (elastic, quasi-elastic, and inelastic) scattering [17,20], NMR spectroscopy [19], and calorimetry [14]. The possibility of exploring in detail the properties of this "biological water" starts with the observation that protein hydration water exhibits the same dynamical fragile-strong crossover (FSC) as that found in confined water and as revealed in Neutron scattering experiments [17]. Figure 2 shows the water mean square displacement (MSD), $\langle x^2 \rangle$, as a function of T and the average translational relaxation time $\langle \tau \rangle$ for lysozyme.

Our goal is to explain the dynamic biopolymer transition on a molecular level by examining the role of water both around and inside macromolecules. In this chapter, we will also make reference to the results we report in Chapter 10 of this volume on the properties of confined water.

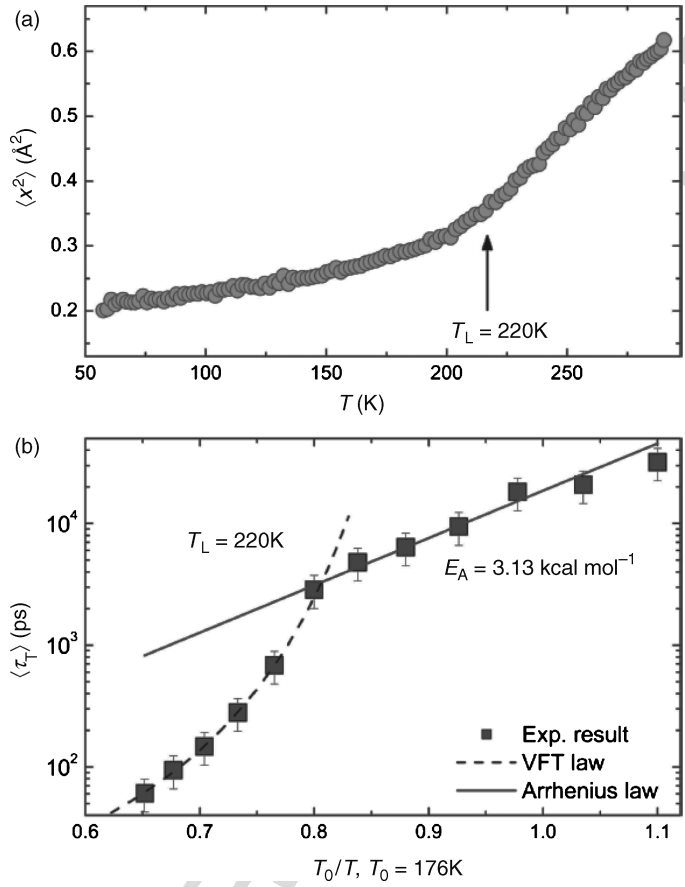

Figure 2. The dynamic transition in lysozyme, neutron data. (**a**) The T-dependence of the mean-squared atomic displacement of the hydrogen atom. (**b**) The average translational relaxation times plotted versus T_0/T (T_0 is an ideal T [17]).

II. THE TWO DYNAMICAL CROSSOVERS

Using the FTIR technique, we map the three main species of water at the protein surface in the range 180K $< T <$ 360K: (i) HB network water, (ii) low-density liquid (LDL) water, and bonded water (HB) with free or non-HB (NHB) molecules. Note that high-density liquid (HDL) is made up of HB and NHB molecules, and is obtained from the thermal evolution of OH-stretching vibrational spectra (OHS) [19,84], the same technique as that used for confined water. The OHS spectra measured for the protein hydration water ($h = 0.3$) reveal significant T-dependences

in the HB and NHB molecules in the presence in the deeply supercooled regime of a spectral contribution assigned to the LDL phase ($\simeq 3100$ cm^{-1}). According to a commonly accepted procedure, this OHS study was done using three Gaussian components related to the LDL phase, the HB component (3220 cm^{-1}), and the NHB water molecules [19]. Note that the LDL contribution is dominant below T_L and the NHB component is dominant at the highest T.

These vibrational bands of protein hydration water show two changes in the population of the three species of oscillators: one at low T at about T_L (the protein dynamical transition and the water FSC) and another at high T (at T_D inside the folding–unfolding reversible region and below the irreversible denaturation). The low-T change occurs when a fraction of the LDL phase (which increases on lowering T) crosses the HB phase (which decreases). The high-T change appears on increasing T when the increasing population of the NHB phase crosses the HB phase. Both results suggest that water drives protein stability and dynamics. In particular, the results suggest that HB formation, and its increasing lifetime or probability with decreasing T, acts like a glue that stabilizes the protein in the range $T_L < T < T_D$ and arrests its dynamics below T_L. A stable HB network involving the protein forms at $\approx T_L$. Below that temperature there is a loss of protein conformational flexibility and, at ≈ 346K (above the second transition), a high percentage of the hydration water molecules are unbonded and the protein unfolds. A combination of FTIR data and NMR data (self-diffusion D and spin-lattice relaxation time T_1) clarifies the role of water in the two protein dynamical transitions. Figure 3 shows the evidence for these two crossovers in the NMR results. Figure 3a shows the inverse of the NMR measured self-diffusion constant D as a function of $1/T$ for $h = 0.3$ and compares it with that of bulk water. The thermal behavior is analogous—in fact, hydration and bulk water follow a Vogel–Fulcher–Tamman (VFT) law ($1/D = A \exp -[B/(T - T_0)]$, where T_0 is an ideal glass transition temperature). For bulk water it is $T_0 = 175$K, and for protein hydration water it is $T_0 = 182$K. In the high-T crossover exhibiting protein conformational change, when T increases, $1/D$ decreases toward the value of pure bulk water. The second crossover takes place at $T_D = 346$K, thus fully confirming the neutron scattering results on the same system [17]. The activation energy of the Arrhenius process in the strong region is $E_A = 3.48$ kcal mol^{-1}, and in the neutron experiment is $E_A = 3.13$ kcal mol$_{-1}$.

To further probe the role of hydration water in the high-T crossover, we measure the NMR proton spin-lattice relaxation time constant T_1 of the lysozyme–water system with $h = 0.3$ in the interval 275K < T < 355K (Fig. 3b). Figure 3b also shows T_1 for pure bulk water. Note that the hydration water T_1 is characterized by two contributions, one coming from the hydration water protons (on the order of seconds, as in bulk water, T_{1h}) and the other from the protein protons (on the order of 10 ms T_{1p}). Figure 3b also shows that, as T increases, the bulk water T_1 follows the VFT law across the entire temperature range, but the T_{1h} exhibits two

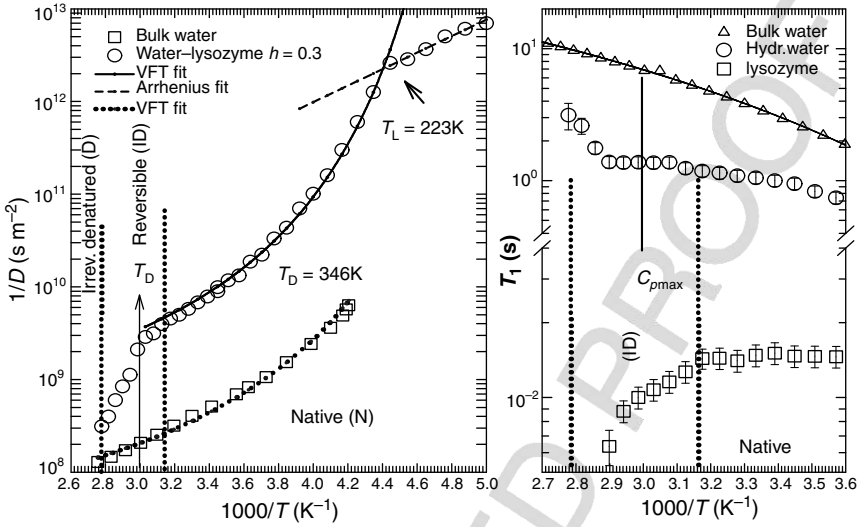

Figure 3. (**a**) The inverse of the NMR self diffusion coefficient $1/D$ versus $1/T$ (squares the bulk water and circles the protein hydration one). The, $1/D$ behavior identifies two crossovers: one at the FSC temperature T_L (223K) and one at a higher temperature (T_D) in the region of the protein denaturation. (**b**) The thermal evolution of the longitudinal NMR relaxation time T_1 [19].

different behaviors, one above and one below the onset of the reversible unfolding regime. Like bulk water, the T_{1h} increases with T in the protein native state, but the T_{1p} of the protein protons remains nearly constant. The situation changes dramatically when T approaches the region of the high-T protein transition: the T_{1p} drops abruptly and disappears at T_D, but the T_{1h} remains nearly constant and then, before irreversible denaturation intervenes, shows a sudden increase toward the bulk water values.

The NMR data are thus consistent with the possibility that the high-T dynamical transition of the protein is driven by the dominance of the NHB fraction of hydration water. At an early stage of reversibility, the protein denaturation process begins when the number of NHB molecules approaches that of the HB molecules, that is, when the probability of a water molecule forming a HB is approximately the same as its forming a NHB.

We next describe the state-of-the-art techniques used to study both dynamical crossovers in such macromolecules of biological interest as proteins, RNA, and DNA. For both crossovers we will consider the related physics by examining experimental findings and MD simulations. Our approach to neutron scattering in biomolecules is essentially the same—with some minor adjustments—as that used in confined water. The mean squared atomic displacement (MSD) $\langle X^2(T)\rangle$ (MSD)

is the quantity used to describe the dynamical properties of biomolecules and their hydration water. We first do a MD calculation on the same quantity. By choosing an appropriate water potential we compare the results with experimental data.

The relaxing cage model (RCM) for neutron scattering is useful in studying both bulk and confined water (see, e.g., Chapter 10). The same technique can be used to describe the properties of biopolymers and their hydration water, in particular the strong dynamic coupling between a protein and its hydration water. The key to this coupling is the FSC phenomenon occurring at approximately $T_L = 225 \pm 5$K in the hydration water. On changing T and P toward FSC, the structure of hydration water transitions from a predominantly HDL form, a more fluid state, to a predominantly LDL form. Neutron data (together with the FTIR and NMR results) provide evidence that this sudden switch in the dynamic behavior of hydration water on Lysozyme, B-DNA, and RNA triggers the so-called glass transition. In the glassy state the biopolymers lose their vital conformational flexibility, resulting in a sharp decrease in their biological functioning.

As mentioned above, incoherent neutron scattering methods—elastic (ENS), QENS, and inelastic (INS)—offer many advantages when studying hydrogen atom dynamics in a protein and its hydration water. The RCM is one good example [21]. In the INS case ($E \neq 0$), the intermediate scattering function (ISF) for a hydrogen atom harmonically bound to a molecule is

$$F_H(Q,t) = \langle \exp[iQX_H(0)] \exp[iQX_H(t)] \rangle \tag{1}$$

where, in the Gaussian approximation, the $\overrightarrow{Q}$ vector pointing in the x-direction in the isotropic sample is [22]

$$F_H(Q,t) = \exp(-Q^2\langle X_H^2 \rangle) \exp[Q^2 \langle X_H(0)X_H(t) \rangle] \tag{2}$$

where $\exp(-Q^2\langle X_H^2 \rangle)$ is the Debye–Waller factor (DWF) that produces the ENS, and the second factor involving the $X_H(t)$ correlation function gives rise to the INS. In the classical regime, $F_H^{cl}(Q,t) = \exp[(-1/2)Q^2W(t)]$.

The $W(t)$ is dependent on the spectral density function $f_H(\omega)$ [22],

$$W(t) = 2V_0^2 \int_0^\infty d\omega \frac{f_H(\omega)}{\omega^2}[1 - \cos(\omega t)] \tag{3}$$

In the case of elastic scattering ($t = \infty$), $\exp[Q^2\langle X_H(0)X_H(t) \rangle] = 1$, and $F_H(Q,t) = \exp(-Q^2\langle X_H^2 \rangle)$, just the DWF. By combining this result with the ISF in the classical regime one obtains

$$\langle X_H^2 \rangle = \frac{1}{2}W(\infty) = V_0^2 \int_0^\infty d\omega \frac{f_H(\omega)}{\omega^2} \tag{4}$$

giving the MSD of the hydrogen atoms as the integral of its reduced spectral density function. From the INS intensity dominated by the incoherent scattering, the Q-dependent vibrational density of states (Q-DOS) of hydrogen atoms can be calculated in the case of protein as

$$G_{\mathrm{H}}(Q, E) = \frac{2M_{\mathrm{H}}}{\hbar^2}\frac{E}{n(E)+1}\langle Q^{-2}\exp(Q^2\langle X_{\mathrm{H}}^2\rangle)S_{\mathrm{H}}(Q, E)\rangle. \tag{5}$$

In the case of hydration water

$$G_{\mathrm{H_2O}}(Q, \omega) = \omega^2 Q^{-2} S_{\mathrm{H_2O}}(Q, \omega) \tag{6}$$

The true hydrogen DOS, $f_{\mathrm{H}}(\omega)$, is thus obtained in the $Q \to 0$ limit of the $G_{\mathrm{H}}(Q, E)$. In the case of water, the $Q \to 0$ limit means $Q < 1\text{Å}^{-1}$, thus $G_{\mathrm{H_2O}}(Q, \omega) = f_{\mathrm{H_2O}}(\omega)k_{\mathrm{B}}T/M_{\mathrm{H_2O}}$.

If we analyze the MSD results, neutron scattering becomes a tool for measuring protein softness. Protein flexibility is essential in enzymatic catalysis and other biological functions. Qualitatively, it results from a protein's conformational disorder. More precisely, it is the result of a protein's response to applied forces that maintain biological structure and govern atomic motion in macromolecules [23]. At room temperature T, biological matter is "soft." This softness can be estimated from the displacement X of a given atom in response to a given applied force F. If an atom is bound to a protein by a spring with a spring constant K, then X is given by the Hook law ratio F/K. Thus for a given F/K, the smaller the spring constant K, the larger the displacement X and the softer the biological material. We can calculate the magnitude of K in protein by using the equipartition theorem, which states that the average potential energy $\langle V\rangle$ of the harmonically bound atom is equal to one half $k_{\mathrm{B}}T$,

$$\langle V\rangle = \frac{1}{2}K\langle X^2\rangle = \frac{1}{2}k_{\mathrm{B}}T \quad \text{and} \quad K = k_{\mathrm{B}}\left[\frac{\partial\langle X^2\rangle}{\partial T}\right]^{-1} \tag{7}$$

Thus, K is proportional to the inverse of the MSD T derivative, that is, if we plot the MSD—measured using ENS as a function of T—the steeper the curve, the softer the biological material at a given temperature.

We use different scattering approaches to obtain the MSD $\langle X^2(T)\rangle$ of the hydrogen atoms. One is the "fixed window scan," which is also used to study the FSC. The experiment consists of an ENS measurement with a fixed resolution window of FWHM (e.g., ± 0.8 μeV [24]) in a T range covering the crossover temperature T_{L}. Because the system is in a stationary metastable state at T below and above T_{L}, the measurements are performed by heating and cooling, respectively, at the same heating/cooling rate (e.g., 0.75K min^{-1}), producing identical results. We calculate $\langle X^2\rangle$ from the DWF, and $S_{\mathrm{H}}(Q, \omega = 0) = \exp[-Q^2\langle X_{\mathrm{H}}^2\rangle]$ using a

linear fitting of the logarithm of $S_H(Q, \omega = 0)$ versus Q^2 plot. We can easily calculate $S_H(Q, \omega = 0)$ from the ratio of the temperature-dependent elastic scattering intensity $I_{EL}(Q, T, \omega = 0)$ and its low-temperature limit, $S_H(Q, \omega = 0) = I_{EL}(Q, T, \omega = 0)/I_{EL}(Q, T = 0, \omega = 0)$. Figure 4a shows the elastic scattering intensity I_{EL} as a function of T at $Q = 0.469$ Å^{-1}. Note the sudden decrease in the I_{EL} above ~220K, which implies a sudden increase in the MSD of hydration

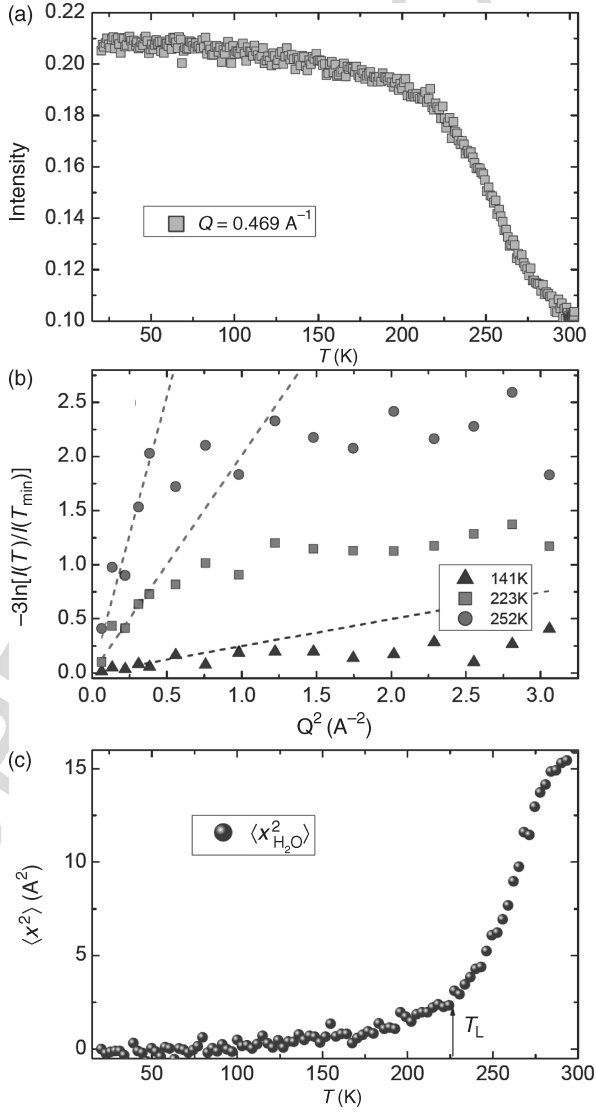

Figure 4. Data analysis method used to obtain $\langle X^2_{H_2O} \rangle$ of RNA hydration water. (**a**) The so-called elastic scan. (**b**) The logarithm of intensity versus Q^2 at three temperatures. (**c**) The extracted MSD of the hydration water as a function of temperature.

water. Figure 4b shows the fitting procedure for three different temperatures ($< T_L, T_L$, and $> T_L$). We plot $I_{EL}(Q, T, \omega = 0)/I_{EL}(Q, T = 0, \omega = 0)$ as a function of Q^2. Because the exponential form of the DWF is a low-Q approximation, only the lowest Q points have been used in the fit to obtain the MSD. Figure 4b shows the linear fit of the lowest five Q values (dashed lines) and Fig. 4c shows the T-dependence of $\langle X^2_{H_20}\rangle$ extracted from the fit.

III. THE PROTEIN GLASS TRANSITION CROSSOVER

A. Neutron Results

Figure 5 shows the results obtained from the RCM in the low-T region of the dynamic crossover (protein glass transition) in RNA. Using a model with the parameters τ_0, β, and γ, we are able to analyze the experimental $S_H(Q, \omega)$ data and calculate the theoretical intermediate scattering function ISF under the condition $\tau_T = \tau_0(aQ)^{-\gamma}$ [21]. The ISF exhibits the two-step relaxation process that is typical of MCT density–density relaxation processes in supercooled glass-forming liquids [25], that is, β-relaxation for the short times and α-relaxation for long times.

We extract the α-relaxation time from the ISFs by taking $1/e$ points for each T (e.g., the arrow in the figure). We also calculate the average translational relaxation time $\langle\tau_T\rangle$. Figure 6 shows the $\log\langle\tau_T\rangle$ versus $1/T$ plot, which enables us to see the dynamic crossover typical in confined water at $T_L = 220$K.

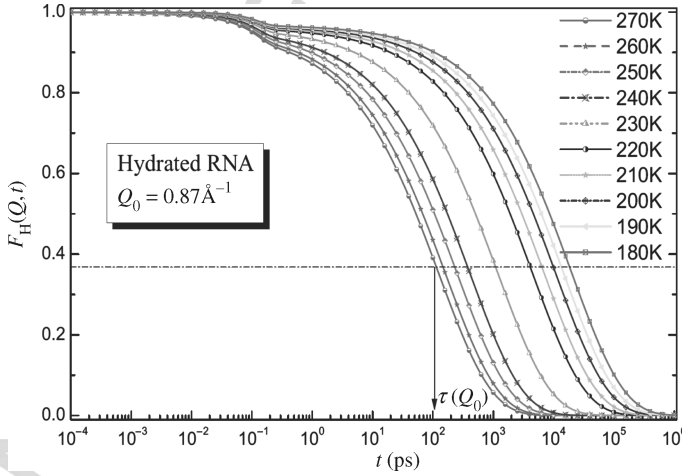

Figure 5. The $F_H(Q, t)$ extracted from the quasi-elastic neutron spectra by using the RCM at Q_0 in RNA hydration water at different T.

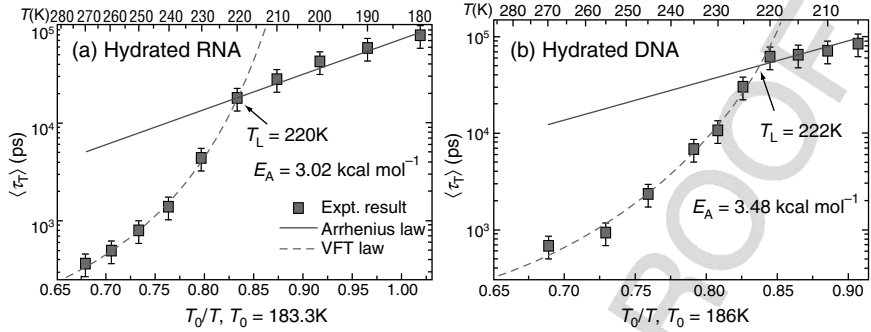

Figure 6. (**a**) The RCM $\langle\tau_T\rangle$ versus T. A dynamic crossover is observed at $T_L = 220$K. The dashed line is the VFT data fit, and the solid line the Arrhenius law. (**b**) A similar analysis for a hydrated DNA where $T_L = 222$K [26].

When $T > 220$K, $\langle\tau_T\rangle$ obeys a VFT law ($\langle\tau_T\rangle = \tau_0 \exp[DT_0/(T - T_0)]$). When $T < 220$K, the $\langle\tau_T\rangle$ transitions to Arrhenius behavior. Figure 6a shows the FSC phenomenon in RNA hydration water (where the activation energy $E_A = 3.03$ kcal mol^{-1}). Figure 6b shows the same plot for DNA hydration water ($E_A = 3.48$ kcal mol^{-1}) [20]. Note that the crossover temperature T_L in both RNA and DNA hydration water is, within error bars, approximately the same.

We use the "fixed window scan" to obtain the MSD $\langle X^2\rangle$ for the same samples. Figure 7 shows the $\langle X^2\rangle$ data taken from the D_2O and H_2O hydrated lysozyme

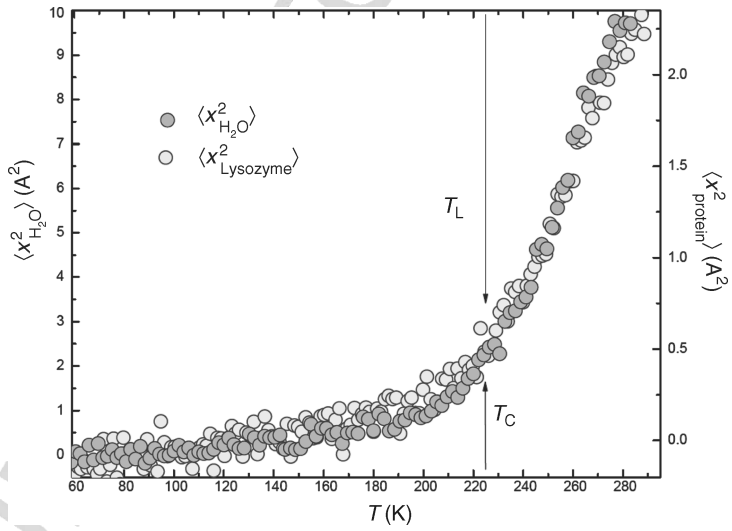

Figure 7. The MSDs measured for the protein (left) and its hydration water (right). The protein MSD is taken from the D_2O hydrated sample.

samples, from which both MSDs from lysozyme $\langle X^2_{\text{lysozyme}}\rangle$ and its hydration water $\langle X^2_{H_20}\rangle$, are extracted, respectively. We multiply $\langle X^2_{\text{lysozyme}}\rangle$ by a factor 4.2 to show the synchronization of the T-dependence of the two MSDs. Figure 7 also shows that the crossover temperatures for both protein and its hydration water are coincident when we define them to be a change of slope of MSD from a low- to a high-T behavior. Note that the crossover temperatures of hydration water (T_L) and the protein glass transition (T_C) agree.

Figure 8 shows the change in softness in both RNA and its hydration water [26]. A biological macromolecule is "soft" at room temperature. Figure 8a shows the MSD of the hydration water molecule, and Fig. 8b shows the MSD of the hydrogen atoms of the RNA biopolymer. The change of slope in MSD of RNA occurs at $T_C \approx 240$K, which is slightly higher than the T_L of hydration water, suggesting that there is a delay in the RNA-induced transition to a more flexible form after the sharp FSC dynamic transition in its hydration water. At the FSC (the locus at which the Widom line is crossed), the relative proportion of LDL to HDL water

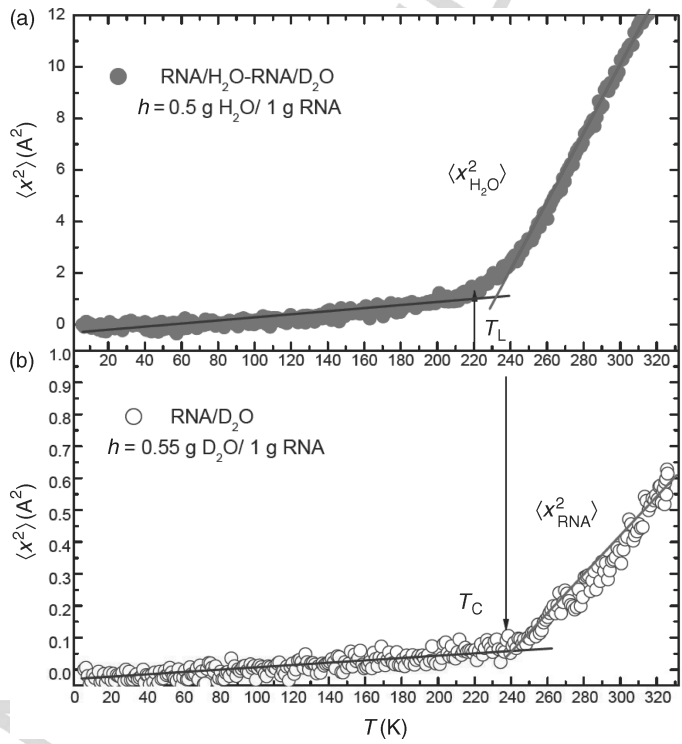

Figure 8. The slope of the MSD versus T curve used as a measure of biomaterial softness. Above the crossover temperature, RNA becomes 15 times softer than its glassy state and hydration water becomes 20 times softer [26].

is about 50:50. The high concentration of partially bonded water that occurs at 20K after crossing the Widom line enables the hydration water to restore RNA activity (or protein-like activity as in lysozyme). The hydrated lysozyme and RNA data show that the dynamic crossover of the hydration water triggers the protein glass transition. Note that when crossing T_L the softness of RNA and its hydration water increase by a factor of 15 and 20, respectively. When we compare Fig. 7 with Figs. 8 and 9, we see that the dynamic crossover is cusp like in the $\langle \tau_T \rangle$ case, and thus it defines T_L more accurately than the MSD.

Note that the pressure dependence of the protein MSD and the corresponding softness has not been as extensively investigated as that at ambient P, although we know that some bacteria can survive under extreme P–T conditions in the deep ocean (e.g., at 1.1 kbar in the Marianas trench). How can microorganism proteins still function under these extreme conditions? High P denatures most dissolved proteins above 3000 bar, and both the structural and dynamic P-behaviors of proteins below the denaturation limit (<2 kbar) affect their biological functioning [27]. Using Monte Carlo (MC) simulation, we observe that the effect of pressure on the hydration water density is key in understanding the cold denaturation of proteins at high pressures [28].

Because neutrons scattered by atomic nuclei are more sensitive to hydrogen atoms than deuterium or other atoms in proteins, and because hydrogen atoms reflect the motions of the side chains and backbone to which they are bound, incoherent neutron scattering experiments on a D_2O hydrated protein can be used to reveal information about protein dynamics in high-P regimes. They show that the T-dependence of protein dynamics follows closely the dynamics of its hydration water under different pressures.

Figure 9 shows ENS results, in particular the calculated MSDs of the hydrogen atoms in the lysozyme molecule $\langle X^2_{\text{protein}} \rangle$ and the hydration water molecule, $\langle X^2_{H_2O} \rangle$, measured by ENS in the low-T range of 40–290K under six different pressures up to 1600 bar. The data are rescaled by a factor of 4.2 to show the synchronization in the T-dependence of the two MSDs at each P. The T-dependence of the MSDs of lysozyme and its hydration water follows the same trend. The linear behavior of each MSD is close to zero at lower T with a very small slope, indicating that the force constant K is very large and the protein rigid. For $T > T_D$, the slope abruptly increases and the K value is approximately 10 times smaller. Because the protein is approximately 10 "softer" than its "glassy" state, its flexibility and ability to function is restored. Note that the T-dependent behavior of the MSD of the lysozyme molecules and their hydration water are visually the same, implying that the dynamic behavior inside the protein is closely related to the dynamic behavior in its hydration water. As in confined water, the dynamics of the hydration water is P-dependent and strongly affects the dynamic behavior inside the protein. Thus, hydration water plays an essential role in protein dynamics. To summarize, ENS experiments indicate that the dynamic transition temperature of the protein

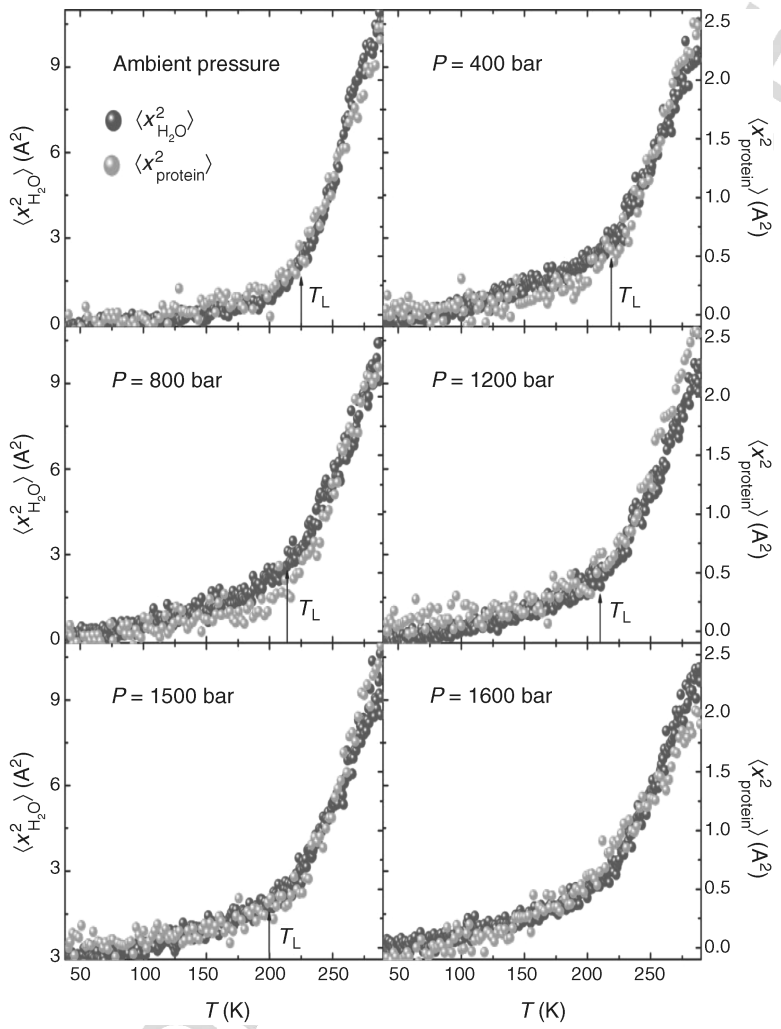

Figure 9. Reduced plot of pressure dependence of MSD of protein and its hydration water [29].

$T_D(P)$ coincides with that of its hydration water $T_D(P) = T_L(P)$ (with the same indication coming from the average α-relaxation time $\langle\tau_T\rangle$ in the hydration water). We, thus, find a dynamic crossover in hydration water at a "universal" temperature $T_L = 225 \pm 5$K in the three biomolecules—lysozyme, B-DNA, and RNA—that can be described as a fragile-to-strong dynamic crossover. Since this dynamic crossover in water is also observed in other substrates (1D confinement in silica porous material and 3D confinement in cement [30]), it appears to be universal

in confined water and one of the dynamic properties of water itself. The dynamic behavior in the protein is thus controlled by the dynamics of its hydration water.

These neutron data strongly indicate that, under pressure, the relaxation time of water molecules is shortened and hydrated proteins remain soft at lower T. Increasing P up to 1500 bar in this low-T region can have the same effect on the relaxation time as increasing T. This faster motion in the relaxation and fluctuation of hydration water under pressure enables the protein to sample more conformational substrates and become active at lower temperatures. Moreover, the dynamic crossover in the $\langle \tau_T \rangle$ of protein hydration water from super-Arrhenius to Arrhenius behavior at a temperature $T_L(P)$ decreases with P. This phenomenon is the effect on the water structure of hydrophobic sites. On the other hand, previous research has shown that applying pressure can also induce an increase in protein–water interactions and improve water accessibility to the hydrophobic core of the protein. In this context, the results of high-resolution quasi-elastic neutron scattering spectroscopy in H_2O hydrated double-wall carbon nanotubes DWNT [31] are of interest. The measurements are made in the temperature range 250–150K and the RCM is used to analyze the quasi-elastic spectra.

Figure 10a shows the T-behavior of the extracted average translational relaxation time $\langle \tau_T \rangle$ obtained by fitting the quasi-elastic spectra of water confined in DWNT with an inner diameter 16 Å. It shows a well-defined cusp-like dynamic crossover at $T_L = 190$K. The solid line represents the VFT law fit, and the dashed line the Arrhenius law fit. Figure 10b shows the MSD averaged over all the hydrogen atoms, $\langle X^2 \rangle$, extracted from the DWF measured using an elastic scan with a resolution of 0.8 eV, as a function of T for the H_2O confined in DWNT. When we compare these results with those of supercooled water confined in porous silica material MCM-41 with different pore sizes, we find that the T_L is insensitive to confinement pore sizes, but is sensitive to the pore chemistry, and that water confined in a hydrophobic substrate DWNT has a lower dynamic crossover temperature by $\Delta T_L \approx 35$K than water in hydrophilic silica substrate.

When water is confined in a hydrophobic substrate, it exhibits a lower T_L than water confined in a hydrophilic substrate, and the protein hydration water crossover temperature decreases with pressure. This P effect reflects the increase in the protein–water interaction and the increase in the water's ability to access the protein hydrophobic core [32]. Using UV spectroscopy, similar P effects on the dynamic properties of biomolecules have been studied in β-lactoglobulin [33], which is also a sensitive food protein. These results suggest that these pressure effects on proteins have universality.

B. The Violation of the Stokes–Einstein Relation

If we confine water into mesoporous material of pore size 14 and 18Å in MCM-41-S, the well-known Stokes–Einstein relation (SER) breaks down [82, 84] when the

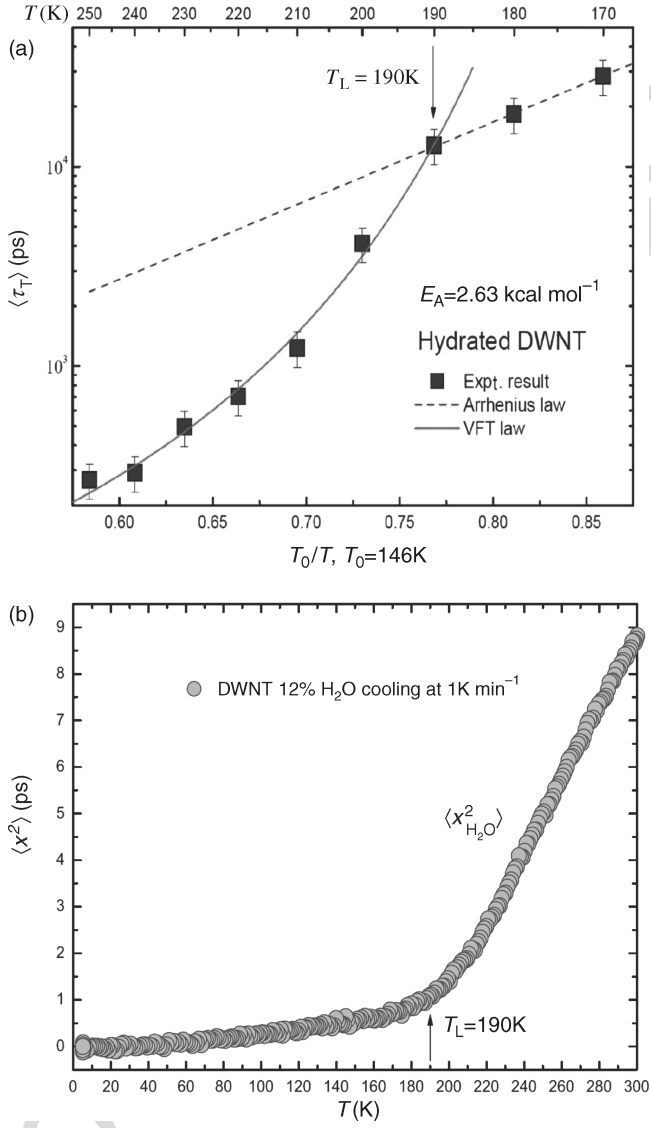

Figure 10. (**a**) The $\langle \tau_T \rangle$ versus $1/T$ of water in hydrophobic nanotubes (DWNT). The solid and dashed lines represent the VFT and the Arrhenius law fits, respectively. (**b**) The MSD versus T averaged over all the extracted hydrogen atoms, $\langle X^2 \rangle$ [31].

average translational relaxation time (or the MCT α-relaxation time) $\langle\tau_T\rangle$ crosses from super-Arrhenius to Arrhenius behavior at $T_L = 225$K (see, e.g., Chapter 10).

The SER in water is $D = (k_B T/4\pi\eta a)[(1 + f)/(1 + 3f/2)]$, where k_B is the Boltzmann constant, η the shear viscosity, $a = 1.44$ Å the effective water molecule diameter, and $f = \beta a/3\eta$ (where β is the slip coefficient at the sphere-liquid interface). Since η is proportional to $\langle\tau_T\rangle$, the product $D\langle\tau_T\rangle/T$ is independent of temperature if the SER is valid. This is indeed the case for $T > 240$K. At the crossover temperature $T_L = 225$K, this product is approximately 10 times larger than the constant value above 240K. The breakdown of the SER causes a fractional SER to emerge in the form $D \sim \langle\tau_T\rangle^{-\xi}$. For strong glass formers, $\xi = 2/3 = 0.67$ for $d = 1$ (one-dimensional confinement), $\xi = 2/2.3 = 0.87$ for $d = 2$, and $\xi = 2/2.1 = 0.95$ for $d = 3$ [34].

The SER breakdown in the protein hydration water (2D confinement) can be observed experimentally from neutron QENS and NMR data. Figure 11a shows $1/D$ versus $1000/T$ measured by NMR [19] and $\langle\tau_T\rangle$ versus $1000/T$ measured by QENS [17]. Figure 11b shows the onset of the fractional SER $D \sim \langle\tau_T\rangle^{-\xi}$. Note in Fig. 11a that at the crossover temperature, T_L ($T_{L,NMR} = 226 \pm 2$K and $T_{L,QENS} = 225 \pm 2$K), $1/D \sim 3 \times 10^{12}$ (s m^2) and $\langle\tau_T\rangle \sim 2 \times 10^4 (ps)$. In the fragile region above T_L, $\xi \sim 1$, indicating that the SER is valid, and in the strong region below T_L, $\xi \sim 0.82 \pm 0.05$, in agreement with the theoretical prediction of $\xi \sim 0.87$ for two-dimensional confined water. The decoupling of D from $\langle\tau_T\rangle$ as seen in the emergence of fractional SER can be attributed to dynamic heterogeneity, which grows to a significant size at and below the crossover temperature.

C. The Simulation Results

Many different experimental techniques indicate the presence of two dynamic transitions in protein hydration water [11,12,17,19,35–39]. The low-T (FSC) dynamic crossover transition at about 225K—the protein "glass" transition—is triggered by the coupling between protein and its hydration water. At the high-T transition associated with the denaturation process, the NHB population dominates, indicating that changes in hydration water accompanies changes associated with protein thermal unfolding. These experiments clearly show that both transitions are connected to the change in the local hydrogen bond pattern of the hydration water, which in turn leads to changes in mobility in both the hydration water and the protein. Note that simulation studies of water in biomolecules are relevant here because they are able to explore complex situations not directly accessible through experiments. The use of MD simulations to study hydration water in biomolecules is appropriate here.

One MD simulation study tests the hypothesis that the observed glass transition in biomolecules is related to the liquid–liquid phase transition of water [40]. It focuses on the dynamic and thermodynamic behavior of lysozyme and DNA

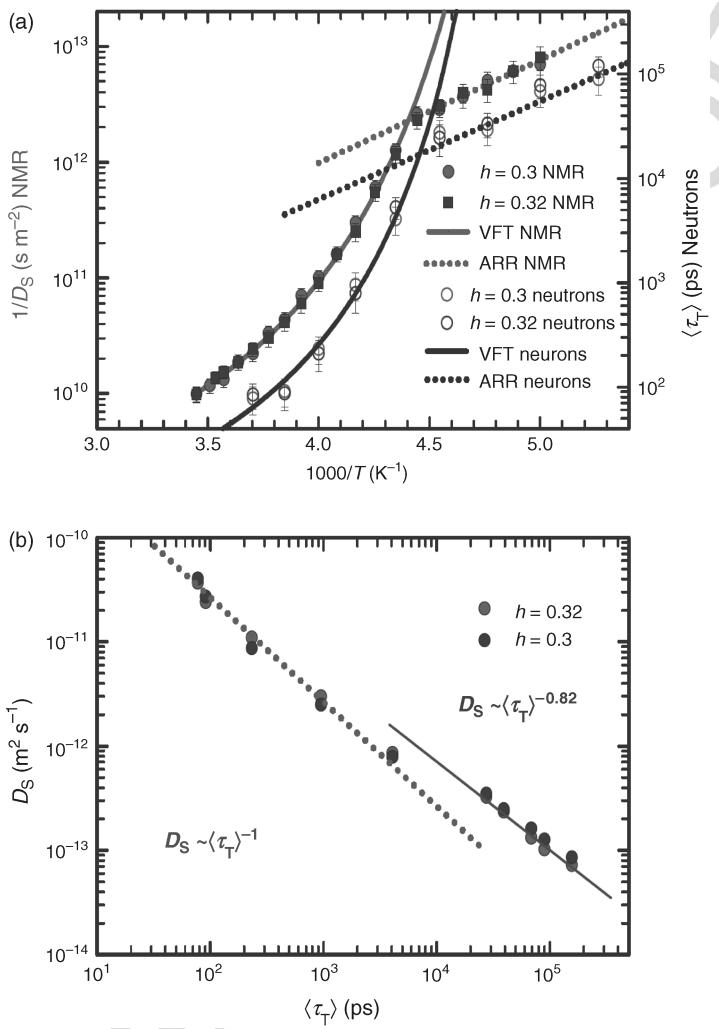

Figure 11. (**a**) The NMR $1/D$ (left) and the QENS relaxation time $\langle\tau_T\rangle$ (right), versus $1/T$. The FSC are at $T_{L,NMR} = 226 \pm 2$K and $T_{L,QENS} = 225 \pm 2$K. (**b**) The scaled SER, $\log D_S$ versus $\log\langle\tau_T\rangle$. Two scaling behaviors above and below T_L are observed: in the super-Arrhenius region $\xi \approx 1$, and in the Arrhenius region $\xi \approx 0.82$.

hydration water, and uses the five-point transferable intermolecular potential of water (TIP5P) and the software package GROMACS [41] to study (i) an orthorhombic form of hen egg-white lysozyme [42] and (ii) a Dickerson dodecamer DNA [43] in a NPT ensemble (constant P, T, and N, number of water molecules) in a simulation

box under periodic boundary conditions. The system equilibration is obtained by means of the Berendsen method. This initial equilibration is followed by a long run, during which the dynamic and static properties (at different T) are calculated. The system consists of a single protein in the native conformation solvated in $N = 1242$ TIP5P water molecules, hence $h = 1.56$. The DNA system consists of a single DNA helix with 24 nucleotides solvated in $N = 1488$ TIP5P water molecules, $h = 3.68$.

The simulation results for the MSD of both protein and DNA find that $\langle X^2 \rangle$ changes its functional form below $T_p \approx 245$K for both lysozyme and DNA. Using numerical differentiation of the total enthalpy of the system (protein and water), C_p has been calculated, by fitting the simulation data for enthalpy with a fifth-order polynomial, and then taking the derivative with respect to T. Figure 12a shows the maxima of $C_p(T)$ at $T_W \approx 250 \pm 10$K for both biomolecules.

The quantitative changes in structure of hydration water can be described in terms of the local tetrahedral order parameter Q [44] for hydration water surrounding lysozyme and DNA. Figure 12b shows that the rate of increase of Q has

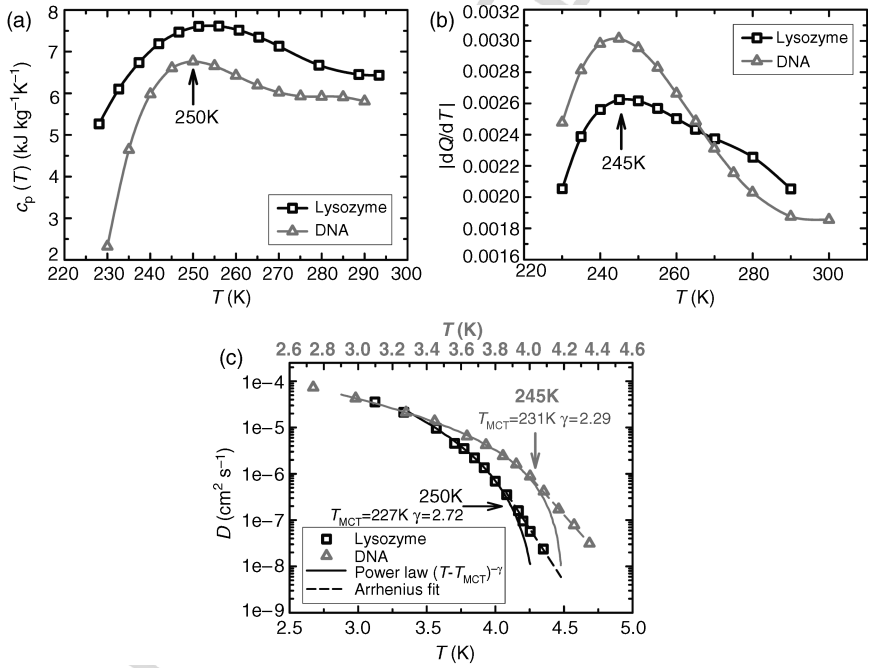

Figure 12. (**a**) The specific heat of the systems lysozyme–water (squares), and DNA–water (triangles). (**b**) The local tetrahedral order parameter derivative, $|dQ/dT|$, for lysozyme (squares) and DNA hydration water (triangles). (**c**) Diffusion constant of lysozyme (squares), and DNA (triangles) hydration water [40].

a maximum at 245 ± 10K for lysozyme and DNA hydration water, the same T as the crossover in the behavior of MSD fluctuations. Finally, upon cooling, there is a dynamic crossover in the diffusivity of hydration water at $T_{cr} \approx 245 \pm 10$K.

The coincidence within the error bars of T_{cr} and T_p again indicates that the behavior of the protein is strongly coupled to the behavior of the surrounding solvent. Note that T_{cr} is much higher than the glass transition temperature, which for TIP5P is estimated to be $T_g = 215$K. That $T_p \approx T_{cr} \approx T_W$ clearly indicates that the correlation between the changes in protein fluctuations and the hydration water thermodynamics implies the possibility that the protein glass transition is related to the Widom line (and hence to the hypothesized liquid–liquid critical point). Crossing the Widom line corresponds to a continuous but rapid transition of the properties of water from local HDL structure to local LDL structure. We, thus, expect that the fluctuations of the protein residues in predominantly LDL-like water (more ordered and more rigid) immediately below the Widom line, will be smaller than the fluctuations in predominantly HDL-like water (less ordered and less rigid) immediately above the Widom line. The agreement in DNA and lysozyme results confirms that the changes in the hydration water are responsible for the changes in biomolecule dynamics. These results are in qualitative agreement with recent experiments on hydrated protein and DNA [20] that find the crossover in side-chain fluctuations at $T_p \approx 225$K.

Other simulation studies have examined such NMR and neutron experimental results as the existence of the two crossovers, especially the crossover in the T region of the folding/unfolding process. Previous efforts sought connections between the FSC observed in hydration water and the crossing of the Widom line, but were not realistic. The simulations on the random powder model reported in Ref. [45] better mimic the neutron and NMR experimental work than the previous protein/water cluster model [40]. In particular, MD calculations agree with the measured temperature dependence of the mean-square hydrogen atom displacements of the protein and its hydration water, $\langle X^2 \rangle$, for example, the inverse of the self-diffusion constant, $1/D$, and the translational α-relaxation time of the hydration water, $\langle \tau_T \rangle$. These comparisons allow us to demonstrate that the experimentally observed dynamic crossover can be attributed solely to the long α-relaxation time of a typical water molecule [46,47], which is also signals the crossing of the Widom line in 2D confined water. At high T, the HDL form dominates and the water structure is fragile. At low T, and upon crossing T_L, the LDL form dominates and the water structure and behavior is strong. This sudden change in the mobility of hydration water at T_L triggers the dynamic transition in protein [45].

When quantitatively comparing simulation results with experimental data, the choice of force field is crucial. Because our focus is the dynamics of hydration water, we use the widely familiar TIP4P-Ew model. It has a computed self-diffusion constant that agrees well with experimental values and with the T scale (its density maximum is at 274K, only 3K below the correct value) down to 230K. Thus, we

implement a OPLS-AA force field for the lysozyme molecules. This force field used in conjunction with the TIP4P model enables the accurate computation of the free binding energies of the protein inhibitors [48]. Note that the so-called "cluster model" composed of a single protein covered by a shell (thin or thick) of water lacks the characteristic features of the powder protein, is in poor agreement with experimental data [49], and produces serious errors and artifacts for all calculated properties. Thus, a *crystal* model (composed of two proteins) or a *powder* model (composed of eight proteins, either oriented or random) is used instead, and the result is a realistic model that can accurate reproduce neutron scattering data [45,50].

In our new study, we put two randomly oriented OPLS-AA lysozyme molecules and 484 TIP4P-Ew water molecules ($h = 0.3$) in a box. After an energy minimization of 5000 steps with a steep descent algorithm, the system is equilibrated in a NPT ensemble [51]. Many simulations are then performed at different T (in the interval 180–280K, with steps of 10K) with a version of GROMACS [41] compiled in parallel such that each simulation is initiated from the final configuration of the closest T.

Figure 13 shows the calculated MSD values for lysozyme, $\langle X^2_{\mathrm{PH}} \rangle$, and its hydration water, $\langle X^2_{\mathrm{H_2O}} \rangle$ together the corresponding experimental values [17,20].

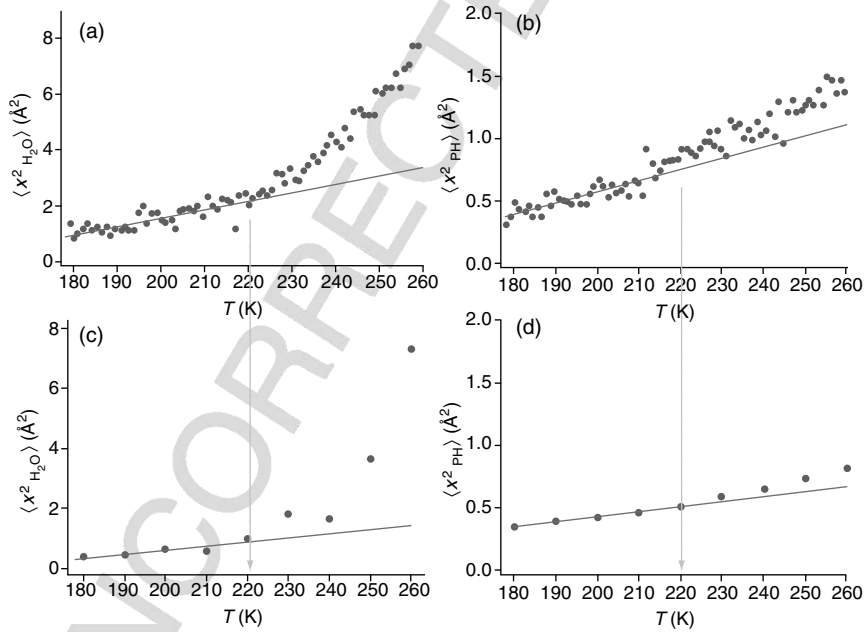

Figure 13. The hydrogen MSD, $\langle X^2 \rangle$, measured by elastic neutron scattering, that is, (**a**) protein hydration water and (**b**) protein hydrogen atoms, and by simulations, that is, (**c**) protein hydration water and (**d**) protein hydrogen atoms [51].

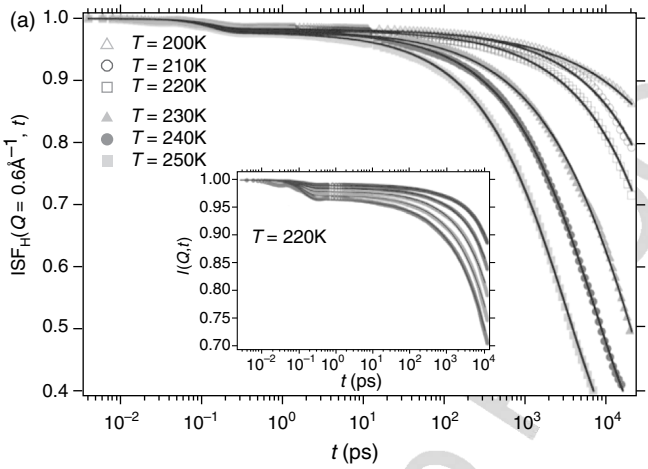

Figure 14. The Water proton incoherent self-ISF calculated at six different T. The ISF at five different Q values (from top to bottom, 0.4, 0.5, 0.6, 0.7, and 0.8 Å^{-1}), inset. The solid curves are fit to the RCM [51].

For all the panels in the low-T regime $\langle X^2 \rangle \sim k_B T$ (straight lines). This behavior extends up to the crossover (T_L and T_C for water and protein, respectively). At the crossover, the slope of $\langle X^2 \rangle$ versus T sharply increases, signaling a change in the dynamics of protein and its hydration water. The crossover takes place at the same T for the MSD of hydrogen atoms both in water and in protein (the arrow signs), implying a strong correlation between the dynamics of hydration water and the protein [45].

Figure 14 shows the calculated ISF for the protons attached to a rigid molecule of hydration water for different T as a function of t at fixed Q value (0.6Å^{-1}). The ISFs are calculated at six different T. The inset shows the ISF at $T = 220$K for different Q values. The solid lines are the best fits to the ISF according to the RCM model and cover the range 2 fs $< t <$ 20 ns. In these ISFs, two contributions are evident: (i) short-t in-cage motion and (ii) long-t cage relaxation (a stretched exponential), that is, α-relaxation, which allows the diffusional motion of the water molecule. Figure 15 shows the plot of the inverse of the hydration water self-diffusion constant $1/D$ versus $1/T$. The inset shows a comparison with the NMR experimental data [19]. The $D(T)$ has been calculated from the trajectories according to the Einstein relation $\lim_{t\to\infty} \langle X(t)^2 \rangle = 2Dt$. The fragile side has been fit with a VFT equation and the result is $T_0 = 169$. The strong side has been fit with an Arrhenius form and the result is $1/D = 142.8 \exp[2086.7/T]$. Note that the calculated crossover temperature $T_L = 225$K and the experimental result $T_L = 223$K are nearly identical.

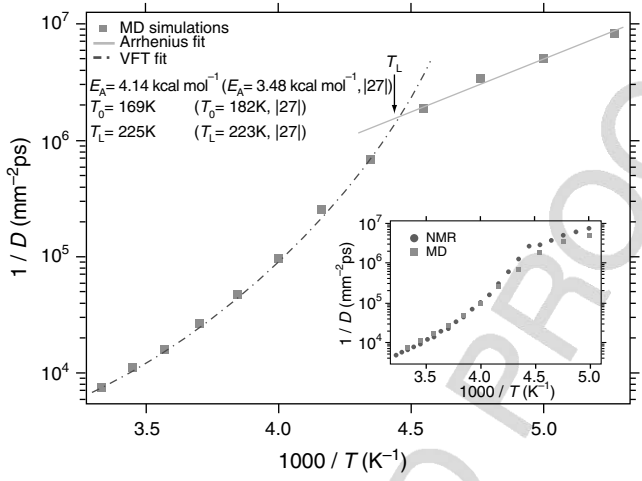

Figure 15. T-dependence of the inverse diffusion constant, $1/D$, from MD simulations. Comparison between MD simulations and NMR data [19] (inset) [51].

Figure 14 shows the extraction of τ_0 from the ISF as a function of T. A Q-independent average translational relaxation time can then be defined as $\langle\tau_T\rangle = \tau_0\Gamma(1/\beta)/\beta$, where Γ is the gamma function and β is the stretch exponent. As previously reported, $\tau_T(Q) \cong \tau_0(aQ)^\gamma$, making the absolute value of $\langle\tau_T\rangle$ dependent on the value of the parameter a, which is chosen to fit the quasi-elastic spectral line shape. Figure 16 shows that the crossover feature is clearly visible at the decay, $\langle\tau_T\rangle$, of the ISF. In the case of $1/D(T)$, the fragile part is fit with a VFT expression with $T_0 = 182$, and the strong part with an Arrhenius law, $\langle\tau_T\rangle = 5.0\exp[1704/T]$. The $T_L = 221$K value is very close to the neutron experiment value 220K [17]. Note that, by considering the value obtained by the $1/D(T)$ fit, we can locate the crossover at $T_L(MD) = 223 \pm 2$K, which is in remarkable agreement with $T_L(\text{exp}) = 222 \pm 3$K. The inset shows a comparison between MD simulation and QENS data [17]. The difference in the absolute scale is due to the different choices of the parameter a ($a_{MD} = 1$ Å, $a_{exp} = 0.5$ Å) in the equation relating $\tau_T(Q)$ and τ_0 in the fitting process.

In summary, using MD simulations we find that the low-T crossover phenomenon is due to the average translational motion of the protein hydration water molecules. The quality of the reported results in the MD simulation of biological systems and their hydration water, and the special agreement with the experimental data, have stimulated further MD research activity. One example is a consideration of the hydration-level dependence of the dynamic crossover phenomenon. How does the relative amount of water hydrating the protein powder affect its dynamics? To answer this, h was increased from $h = 0.3$ to $h = 0.45$ and $h = 0.6$

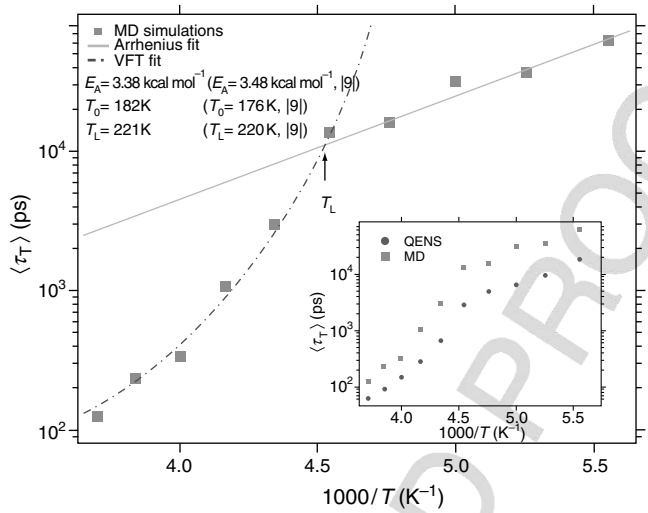

Figure 16. T-dependence of the average translational relaxation time, $\langle\tau_T\rangle$, from MD simulation [51]. Comparison between MD simulation and QENS data [17] (inset).

and it was found that the first hydration layer ($\sim$ 2 Å from the protein surface) is approximately 15% more dense than bulk water, but that the normal density is recovered in the second hydration layer ($\sim$ 4.5 Å) [52]. We can, thus, expect that as the values move from $h = 0.3$ to $h = 0.6$ the water properties will more closely resemble those of bulk water. This has been confirmed by the behavior of the calculated ISFs. From both their T-dependence and Q-dependence at $h = 0.45$ and 0.6 we see that, as h increases, the dynamics become more rapid. The water–water interactions are less strong than protein–water interactions, thus the bulk water limit corresponds to minimum relaxation times. As h increases (i) the average α-relaxation time decreases, (ii) the crossover temperature T_L decreases, and (iii) the activation energy E_A of the Arrhenius part decreases. This confirms that the bulk water case is a limit case.

D. About the FSC

It was recently suggested that the crossover observed at T_L is caused when finite-sized materials confine liquid molecules, a hypothesis that has emerged from observations of viscosity changes in liquid molecules [53]. The relaxation in glass-forming liquids is described by the α (characterized by a VFT T-dependence) and β (Arrhenius) processes, and specifically from such corresponding transport parameters as relaxation time (τ) and viscosity (η). We can typically use the η-related α and one or several secondary β relaxation processes. The α relaxation of confined water vanishes at the T at which the volume of water clusters become larger

than the volume of the confining geometries, and this makes extending cooperative relaxations difficult. This typically occurs around T_L. Above T_L we observe a merged α–β relaxation, and below T_L only a local (β) relaxation. Note that this does not mean that a real FSC cannot occur in bulk (or bulk like) water where the α relaxation is observed in the deeply supercooled regime.

Dielectric spectroscopy and scattering studies on the structural relaxation in many different materials have assumed that the "normal" T-dependence of the relaxation time of a liquid will closely resemble that of propylene glycol (PG), that is, both bulk water and confined PG relax in the same manner, and with an apparent continuity. The main relaxation time of PG exhibits a thermal behavior that differs from that proposed for bulk and confined water. Confined water relaxation times seem substantially altered when compared to bulk water (which evidently is not the case in confined EG). It also shows an apparent FSC. In addition, an even more dramatic change in the T-dependence of water confined in nanoporous MCM-41 is clearly evident. These results are not unique in that they simply exhibit the typical behavior of supercooled water in biological materials and in other confined environments. Thus, we consider both bulk and confined ethylene glycol (EG, $OHCH_2CH_2OH$). Figure 17 shows the EG dielectric relaxation times studied.

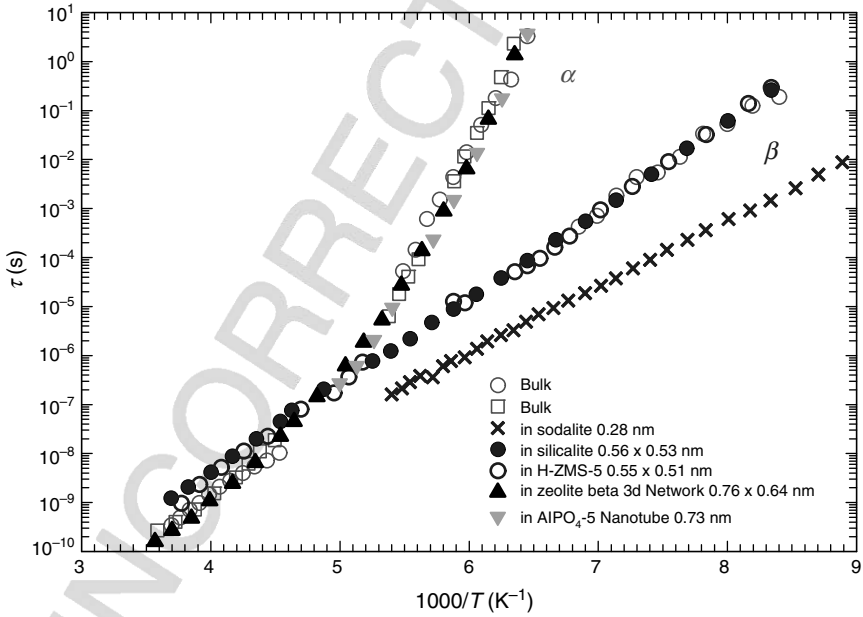

Figure 17. The ethylene glycol (EG), bulk [53,54] and confined in different geometries, dielectric relaxation times (τ) as a function of T.

The bulk data come from two different experiments [53,54] and all the confined EG results have been individually measured [54] in different confining geometries: sodalite (0.28 nm), silicalite (0.56 nm $\times$ 0.53 nm) and H-ZSM-5 (0.55 nm $\times$ 0.51 nm) pores, zeolite beta 3D network (0.76 nm $\times$ 0.74 nm), and $AlPO_4$-5, a nanotube with a diameter of 0.73 nm.

Figure 17 shows a crossover between two thermal behaviors in both bulk EG and EG confined in a zeolite beta 3D network and $AlPO_4$-5 nanotubes. When alcohol is trapped in cages with a pore diameter less than 0.6 nm, the severe confinement induces "strong" behavior at all T studied. Note that the relaxation times for EG in sodalite are significantly slower than those in silicalite or H-ZSM-5. The behavior of supercooled liquids is typically characterized by two relaxations: (i) a local relaxation (covering the short-time regime of single molecule dynamics) and (ii) a cooperative relaxation (covering many temporal orders of magnitude). In this second case, the corresponding density fluctuations are due to a certain number of molecules interacting on a characteristic length scale ξ that is larger than the molecular size a_0. When the liquid is severely confined, that is, when the typical confinement length l is $l \ll \xi$ (i.e., is a "cage" of a few molecules or even one molecule), only local relaxation survives. On this basis, and taking into account only the τ data behavior of bulk EG and EG confined in silicalite and H-ZSM-5 (a severe confinement), it has been proposed that the crossover observed in supercooled confined water is only an apparent FSC, and that in reality it is due to a merged α–β relaxation at high T and is a pure β relaxation below the apparent transition. Thus, after incorporating such considerations regarding the water physics as the estimation of T_g, we conclude that (i) in contrast to other liquids in similar confinements, confined supercooled water does not exhibit a true glass transition, and (ii) this implies that deeply supercooled water in such biological systems as membranes and proteins usually exhibits only a local β relaxation. This important point alters our understanding of the low-T properties of biological materials.

Note that Fig. 17 shows (i) that α-relaxation is present at all T in bulk EG as well as in EG confined in a zeolite beta 3D network and $AlPO_4$-5 nanotubes, (ii) that the $\tau(T)$ data indicate a well-defined crossover at $\approx$ 200K in which the EG molecules confined in the $AlPO_4$-5 nanotube interact the same (via HBs) as water molecules confined in MCM-41, and (iii) that the EG molecular size is $a_0 \sim 5.5$ Å (more than double that of water). Thus, if EG confined in a nanotube with pore diameter 0.73 nm (the $AlPO_4$-5) can maintain its α-relaxation, why must water $a_0 \sim 2.2$ Å confined in a 1.8 nm MCM-41 pore pass from α-relaxation to pure β-relaxation? If the intermolecular interactions are of the same type and if, in the EG case, only few interacting molecules are needed to cause α-relaxation, then analogous considerations should also hold for water.

Figure 18 shows the relaxation times measured—using a series of different experimental techniques—in bulk and in confined water, confirming that FSC

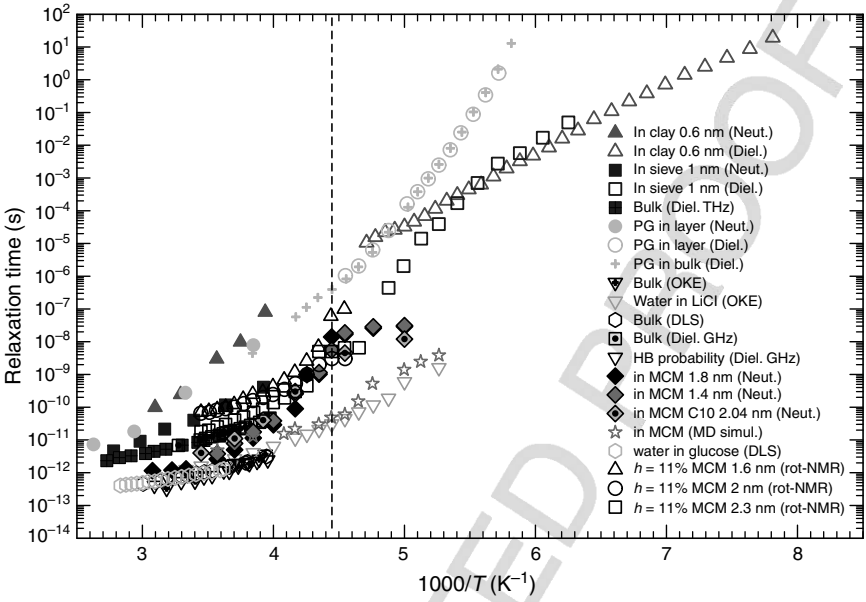

Figure 18. Relaxation times versus $1000/T$, measured for water in bulk [55–58] and in confining geometries [59–68]. Propylene glycol data are also reported [69,70]. Dashed line indicates T_L.

occurs in confined water. Also included are PG data [53,69,70]. Figure 18 shows the relaxation times of bulk water [55–58,67] and of water in a variety of confining geometries (and solutions), that is, water confined in clay [59], in a sieve [60,61], in MCM-41 [62], in MCM-C10 [63], in the MD simulation of MCM [64], in solution with glucose [65], and on the surface of MCM $h = 0.11$ in an experiment of quadrupole rotational NMR or deuterons T_1 [66]. The solid symbols indicate neutron scattering and the open symbols indicate the dielectric optical Kerr effect (OKE), depolarized light scattering (DLS), and NMR. Note that all experimental τ data on confined water show a crossover. Although the bulk water relaxation time measured using dielectric relaxation differs by approximately one order of magnitude from that measured with light probes DLS and OKE, it appears that the NMR technique agrees with the neutron technique. These τ differ according to the techniques used. Experiments that probe rotational or rototranslational motion are more sensitive than those that probe translational dynamics only [81]. In addition, water confined on a surface (e.g., lysozyme and MCM) has τ values two orders of magnitude slower with respect to light data. The τ data measured using the dielectric technique differ from τ data measured using light scattering because DLS, unlike dielectric spectroscopy, probes the HB time directly.

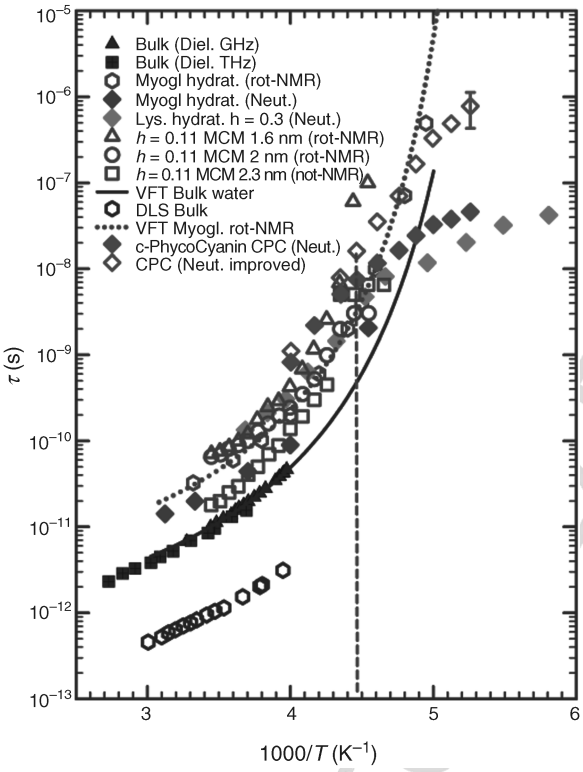

Figure 19. The relaxation times (τ vs. $1000/T$) of different protein hydration water, surface water of MCM-41, and bulk water. The dashed line indicates T_L.

We now show that crossovers are also found in protein hydration water by examining corresponding relaxation times in different biomolecules and comparing their T-behavior with that of pure bulk water. Figure 19 shows the relaxation times of lysozyme, myoglobin, and C-PhycoCyanin hydration water, and compares the data with data for water on the surface of MCM-41 [66], for bulk water (measured using DLS [57], and for dielectric spectroscopy (in the GHz and in the THz range) [55,58]). Also shown are protein hydration water data for myoglobin (rotational-NMR [71] and neutrons [72]), lysozyme (neutrons [17]), and C-PhycoCyanin (neutrons [73]). The behavior of lysozyme hydration water ($h = 0.3$, i.e., a single layer) is nearly coincident with that of the MCM sample with an hydration level $h = 0.11$ where all the water molecules are on the internal surface of the tube. Note also the VFT fit of the pure bulk water data (solid curve) and of the rotational NMR data of myoglobin hydration water (dotted curve). We see a dynamic crossover in all the data. Note that, prior to the crossover ($T > T_L$), the $\tau(T)$ behavior as a function of T coincides, within the error bars, to that of bulk water (see, e.g., the two approximately identical VFT curves).

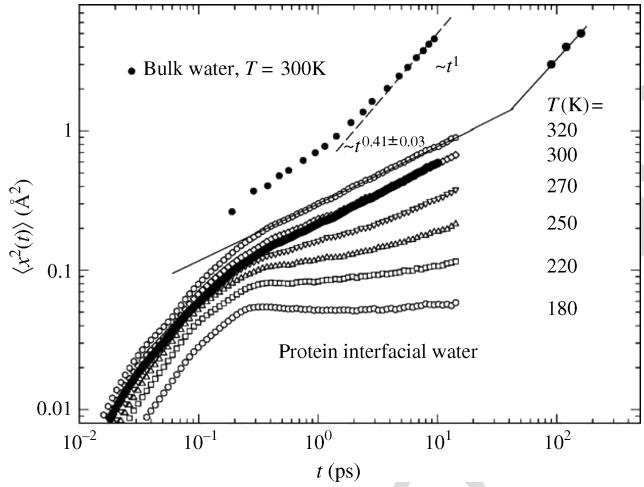

Figure 20. The time-resolved MSD ($\langle x^2(t)\rangle$ vs. t) of bulk water and of myoglobin hydration water ($h = 0.4$), measured by neutron for 180K < T < 320K [71].

Figure 20 shows the time-resolved MSD ($\langle x^2(t)\rangle$ vs. t) of bulk water and of myoglobin hydration water ($h = 0.4$) measured using neutron scattering [71]. Each curve corresponds to a temperature in the range 180K < T < 320K. The behavior of $\langle x^2(t)\rangle$ versus t depends on the diffusional motion $\langle x^2(t)\rangle = 2Dt^{\gamma}$. When $\gamma = 1$ the dynamics are Brownian, but when $\gamma \neq 1$ the dynamics become fractal like, that is, with different probabilities they take "flight" and move from one cluster to another. We see different $\langle x^2(t)\rangle$ curves for different T. When $T = 180$K the $\langle x^2(t)\rangle$ curve is nearly flat (with $\gamma \sim 0$ in the picosecond region), indicating that water molecules are trapped on the protein surface in a glass state. When T is increased, a dynamic change occurs at $T > 220$K. Increasing T further we see a dynamical evolution that differs from the behavior of bulk water.

IV. HIGH-TEMPERATURE DYNAMIC CROSSOVER

A. Neutron Scattering and MD Simulation Results

As previously reported, lysozyme under thermal unfolding [13–15] exhibits intermediate structures. (These can also be induced by pressure and chemical changes [74].) Its unfolding process is thus a three-state model $N \rightleftarrows I \longrightarrow U$. Reversible denaturation, a FSC associated with the configurational entropy change [75], is the first step. The second is irreversible denaturation, which is due to the association of unfolded lysozyme units [76].

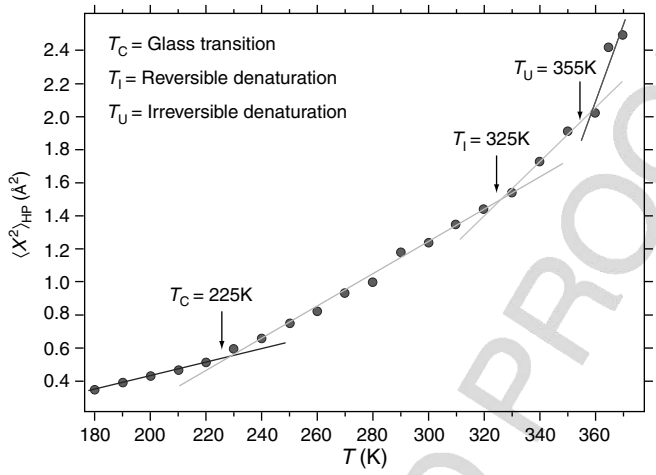

Figure 21. $\langle X^2 \rangle_{HP}$ as a function of T for protein hydrogen atoms calculated from MD simulations [74].

The reversible step may be related to the dynamic crossover in protein hydration water at $T_D \approx 345 \pm 5$K. NMR self-diffusion results [19] indicate that at this temperature a sudden change in hydration water dynamics occurs and the inverse diffusion constant switches from low-temperature super-Arrhenius behavior to high-temperature Arrhenius behavior. Neutron techniques (QENS) have also been used to study protein hydration water at this high-T crossover. Figure 21 shows the atomic MSD of protein hydration water at the low-T crossover measured using MD simulation. These crossovers can also be shown theoretically. Whenever the slope of an Arrhenius plot of the $D(T)$ changes, the specific heat has a peak. The well-known Adam–Gibbs equation (AGE) shows this as

$$D = D_0 \exp(-C/TS_{\text{conf}}) \tag{8}$$

where D_0 is a prefactor, C is a constant, and S_{conf} is the configurational entropy. If we assume that the AGE is also valid at high T for hydration water, the specific heat peak observed using calorimetry during lysozyme thermal denaturation [14] will agree with the NMR data, that is, there will be a high-T crossover phenomenon for the inverse of D [19].

This picture is confirmed when we measure the chemical shift δ in the NMR data to get $C_{P,\text{conf}}$ [15]. In lysozyme it has been also found that the contribution of the configurational disorder to entropy is dominant, so $S_{\text{conf}} \approx S$ and

$$S_{\text{conf}}(T) \approx S_{\text{conf}}(0) + \int_0^T C_P \mathrm{d}T/T \tag{9}$$

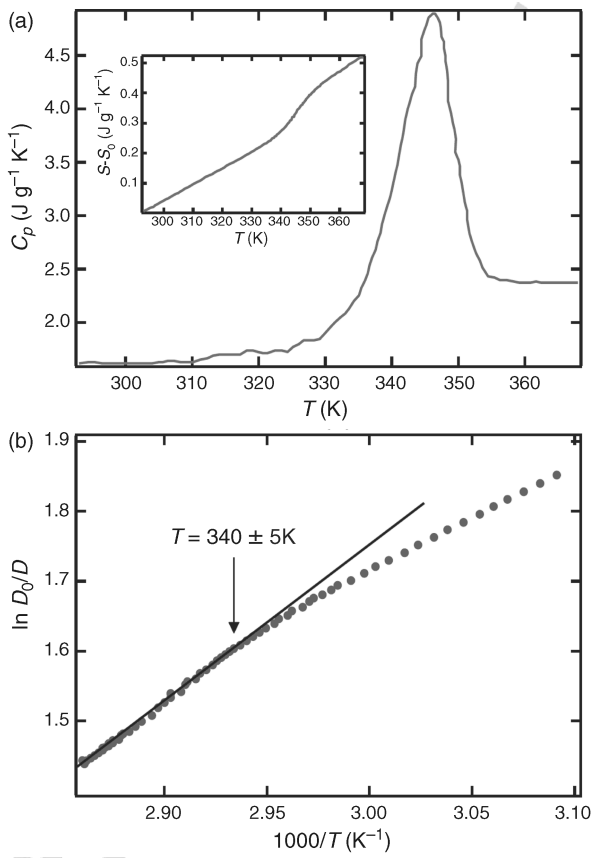

Figure 22. (**a**) Experimental C_P of a water–lysozyme solution [14] Inset: $S(T)$ versus T calculated from integration of the experimental C_P. (**b**) Arrhenius plot of D_0/D versus $1000/T$ obtained according to the Adam–Gibbs equation [74].

a law valid at low T in the supercooled region of water [77,78]. Figure 22 shows a numerical example, an Arrhenius plot of the resulting D_0/D as obtained by substitution in the latter equation of C_p reported in Ref. [14]. The plots of both entropy and D_0/D show a kink at 340 ± 5K, corresponding approximately to the maximum in the $C_{P,\mathrm{conf}}$.

We now consider $1/D$ and migration distance d of the hydration water molecules extracted from QENS spectra. We compare the QENS result with several quantities calculated using MD simulations, for example, $1/D$, the protein backbone root mean square displacement (RMSD), the hydrogen bond relaxation time τ_{R}, and the protein hydrogen atom MSD $\langle X^2 \rangle$. Together these quantities indicate a change in the water–lysozyme hydrogen bonding in the range 330K $< T <$ 345K. Using calorimetric and FTIR measurements, the same 330K $< T <$ 345K range is found for the reversible conversion of $N \rightleftarrows I$ in lysozyme solutions.

We use the experimental and MD methods associated with the low-T dynamic crossover ($T_L \approx 220$K) to probe the QENS experiments. The high-resolution (approximately 3.5 μeV, FWHM) backscattering spectrometer BASIS at the Spallation Neutron Source, the most intense pulsed neutron source in the world, was used to measure the diffusive motion of lysozyme hydration water from $T = 290$ to 380K. The BASIS spectrometer is particularly appropriate for measuring diffusive and relaxational processes on the 10^{-12} to 10^{-9} timescale, and both H_2O hydrated and D_2O hydrated lysozyme samples were considered. The spectra from the contribution of hydration water only are obtained [74]. Because of the very large incoherent cross section of hydrogen atom, QENS experiments provide the incoherent dynamic structure factor $S_H(Q, E)$ of the hydrogen atoms of the water molecules in the protein hydration layer. The measured neutron intensity at each Q

$$I(Q, E) = A\{p(Q)\delta(E) + [1 - p(Q)]S_H(Q, E)\} \otimes R(Q, E) - BG \qquad (10)$$

where A is the normalization factor, $p(Q)$ is the elastic scattering component related to quasi-static scatterer, $R(Q, E)$ is the energy resolution function, and BG is the nonlinear background properly processed.

$S_H(Q, E) = S_T(Q, E) \otimes S_R(Q, E)$, that is, a convolution of the translational dynamic structure factor, $S_T(Q, E)$, and the rotational one, $S_R(Q, E)$. In addition, for small Q spectra, $Q < 1$ Å^{-1} the $S_R(Q, E)$ can be made negligibly small, hence $S_H(Q, E) \simeq S_T(Q, E)$ and its Fourier transform will give the self-intermediate scattering function $F_H(Q, t)$ that have a stretched exponential $F_H(Q, t) = \exp[-\Gamma(Q)t]^\beta$ long-time decay. When the T is above the room temperature, $\beta \simeq 1$. A situation for which the exponential form $F_H(Q, t) \approx \exp(-\Gamma(Q)t)$ can be approximately used, or equivalently, in frequency domain the $S_H(Q, E)$ of water is approximated as a Lorentzian shape function [67],

$$S_H(Q, E) \approx S_T(Q, E) = \pi^{-1}\Gamma(Q)/(E^2 + \Gamma(Q)) \qquad (11)$$

where $\Gamma(Q)$ is the half width at half maximum (HWHM). Its validity can also be confirmed by the good agreement between the experimental data and the fitted curve with the model for all T and wave vector transfers. In the $Q \to 0$ limit, it is well known that $\Gamma(Q) = DQ^2$, where D is again the water translational self-diffusion constant. Thus for the finite, but small Q, we may take into account the next order correction to the Q^2 dependence as

$$\Gamma(Q) = DQ^2(1 - \xi^2 Q^2 + L) = DQ^2(1 + \xi^2 Q^2) \qquad (12)$$

From the inverse of this equation: $1/\Gamma(Q) = (1/D)((1/Q^2) + \xi^2)$, a plot of $1/\Gamma$ versus $1/Q^2$ will give a straight line with a slope $1/D$, a good approximation. In addition, $\xi^2 \simeq D\tau_0$, where τ_0 is the average time duration that a water molecule spends oscillating in a cage forming by its nearest neighbors [67].

In the dense liquid state near the room temperature, a water molecule is first trapped in a site for a time interval τ_0, on the order of 0.1 ps, oscillating in a cage formed by adjacent water molecules connecting by hydrogen bonds. The hydrogen bonds are continuously breaking and reforming. After the time τ_0, the cage gradually relaxes, and then the water molecule starts to move away from the trapped site for a time interval τ_1, until it gets trapped again in a new site. However, the cage relaxation time τ_1 is not necessarily much less than τ_0. It depends on the temperature of water and can be, as observed in the many cases of confined water here presented, on the order of ps to ns at low T.

After extracting D, according to the described procedure, one can then plot D/Γ versus $1/Q^2$. The result is a set of parallel straight lines with a zero intercept ξ^2 that can thus be extracted with tolerable accuracy. So, one can finally calculate the characteristic migration distance between successive traps of water molecules using ξ^2 as

$$d = \sqrt{\langle l^2 \rangle} = \sqrt{6\xi^2} \tag{13}$$

It is a measure of the average distance that a water molecule travels between two successive traps. While D represents how fast a molecule diffuses, the migration distance d represents how far the center of mass of a typical molecule translates in the cage relaxation process, before it gets trapped again. The measured data of $1/D$ and d are reported in Fig. 23. Figure 23a shows an evidence of an Arrhenius to super-Arrhenius dynamic crossover as T is raised across $T_D = 345 \pm 5$K. Below T_D, the inverse diffusion constant can be fitted with the VFT law with $T_0 = 204 \pm 3$K and $C = 0.94$. While above T_D, the inverse diffusion constant can be fitted with the Arrhenius Law $1/D = 1/D_0 \exp(E_A/RT)$ with $E_A = 5.97 \pm 0.55$ kcal mol^{-1}, which corresponds to about an energy needed to break 2.4 hydrogen bonds at T_D [79]. Figure 23b shows the extracted d, that is the migration distance of the water molecules between two successive trap sites. One can see that it is increasing slowly below T_D, from 4.2 to 5.6 Å, but rises sharply above T_D to 9.6 Å at 380K. The result is consistent with the literature results 6–9 Å at room temperature. The sharp changes of both the self-diffusion constant D and the migration distance d indicate a large-scale enhanced movement of the water molecules above the crossover temperature T_D, when the lifetime of the HB network of the water molecules becomes shorter, and thus it is not able to maintain the shape of the protein.

The protein powder model discussed for the low-T crossover, was thus used to analyze measured QENS spectra of the protein hydration water for temperatures ranging from 290 to 380K, covering the first stage of the denaturation process, occurring at the reversible protein denaturation temperature around 345K. In joint was also developed a MD simulation study for the same process, the main obtained results are exposed in the following. Details are the following: lysozyme

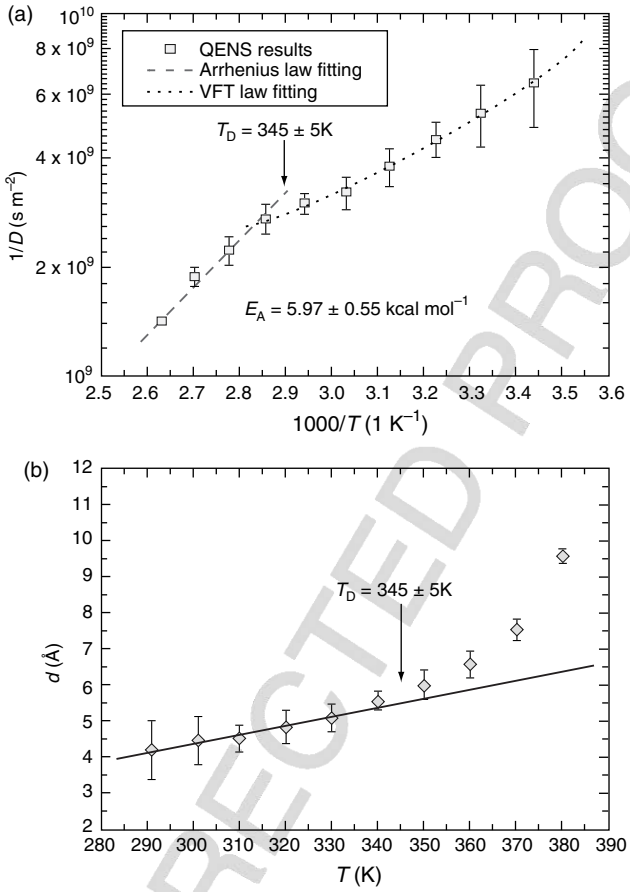

Figure 23. (**a**) The plot of experimentally extracted $1/D$ versus $1000/T$ of the protein hydration water shows the dynamic crossover as T is raised through $T_D = 345 \pm 5$K. (**b**) Plot of experimentally extracted average migration distance d of the hydration water [74].

molecules (Protein Data Bank file 1AKI.pdb) randomly oriented are put in a box two OPLSAA29 and 484 TIP4P-Ew water molecule, so that $h = 0.3$ for each protein. Nine simulations were performed at different T (from 290 to 370K, with 10K intervals) with a parallel-compiled version of GROMACS33 by using a triclinic cell (box size ~43 Å× 37 Å× 32 Å); each MD simulation length was 50 ns after the equilibration time. After that the hydrogen bond correlation function was calculated according to $c(t) = \langle h(0)h(t)\rangle \,/\, \langle h(t)\rangle$, where $h(t) = 1$ if the hydrogen bond exists and $h(t) = 0$ otherwise. From the decay of this correlation function one can calculate the hydrogen bond relaxation time τ_R, as the $1/e$ value of $c(t)$.

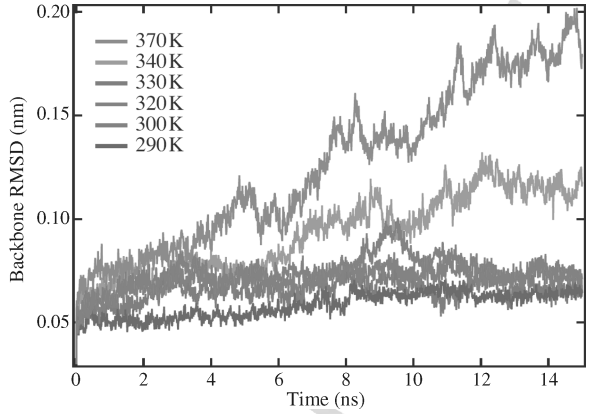

Figure 24. The backbone RMSD as a function of t at different T. No remarkable change is detected until 340K when the protein increases its flexibility [74].

The obtained MD simulation results together with the confirmation of this dynamic crossover in protein hydration water suggest that it may be connected to the first stage of the unfolding process of the protein. The protein backbone RMSD calculated from the trajectories shows a sudden increase between 330 and 340K (Fig. 24), signaling the beginning of the denaturation process.

Molecular dynamics simulations are limited to a t-step on the order of fs, while protein unfolding occurs on timescales of the order of ms. In that cases, atomistic simulations of the whole denaturation process are still far from the conventional computers capabilities, nevertheless, a few ns are enough to capture at least its dynamic beginning. At the same T, the Arrhenius plot of $1/D$ (Fig. 25) obtained from

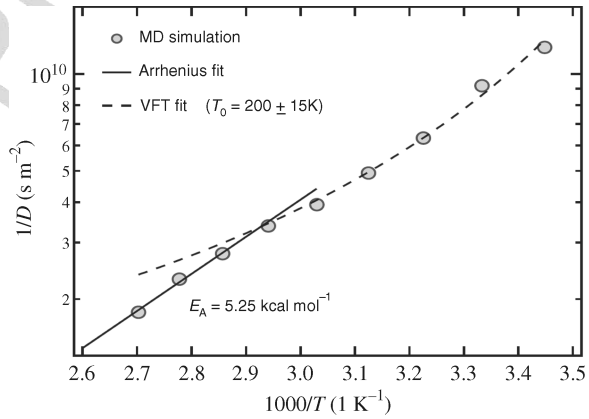

Figure 25. Arrhenius plot of the $1/D$ for lysozyme hydration water, calculated from MD simulations. The curve shows an high-T dynamic crossover similar to the one observed by QENS (Fig. 24) [74].

the MD simulation shows a change in its behavior at $T_D = 340 \pm 5$K, reproducing well the neutron scattering data and qualitatively the AGE.

In particular, the extracted activation energy $E_A = 5.25 \pm 0.5$ kcal mol^{-1} is in agreement with the experimental value ($E_A = 5.97 \pm 0.55$ kcal mol^{-1}). MD simulations have also given some additional suggestions on the underlying physical mechanism for lysozyme reversible denaturation by means of three calculated physical quantities like: the protein hydrogen atoms MSD, the water–protein HB relaxation rate ($1/\tau_T$) and the number of the water–protein hydrogen bonds. In the first case, the MSD has a sharp increase as a function of T at about T_D in agreement with the onset temperature for reversible denaturation determined by calorimetry [14]. At the same temperature T_D, water–protein HB relaxation rate increases and deviates from linearity, signaling the beginning of the breakdown of the HB network around the protein. Such an increase in the HB relaxation rate is the cause of the enhanced protein flexibility, as already pointed out by Wood et al. [80] for the low-T protein dynamical transition, where a correlation between the decrease of protein HB network relaxation time (due to the onset of water translational diffusion) and the sudden increase in the protein hydrogen atoms MSD at $T_L = 220$K, was founded. Here (high-T crossover), the situation is analogous, but with a difference: the solvent cage is not able to constrain the folded protein structure anymore and the macromolecule increases its ability of sampling the configurational space. Due to the decrease of the HB lifetime, its flexibility becomes large enough to start the unfolding process. Finally, as T further increases, the number of HBs between water and the protein has a sharp change in its rate of decrease at $T_D = 340$K, from 0.3 to 1.2HBs K^{-1}.

That is to say, the dynamics of interfacial water and its interactions with the protein surface are critical for the stability of protein structure. As soon as the strength of HBs at the interface between water and protein reaches a certain value, the 2D network around the protein that kept it folded collapses, allowing the macromolecule to increase its flexibility and to begin the denaturation process. We believe that the crossover phenomenon is a characteristic of the whole water–protein system: the decreased interaction at the water–protein interface is the cause of both the crossover and the denaturation. On one hand, water becomes more mobile (increased diffusion constant); on the other, protein is not constrained by the HB network and can unfold.

It is important to stress that the combination of both the low-Q QENS data and MD simulations allows us to understand on a molecular basis the onset of the reversible folding and the successive irreversible denaturation. In particular, by considering these results and the cited NMR and FTIR experimental data [15,19] it is possible to conclude that the denaturation of the protein and the dynamic crossover in its hydration water are causally related. In fact, all of their coincidences suggest that this high-T crossover could be a significant factor in the reversible denaturation process. We also note that the organization of water/biomolecules

constitutes an extremely important research field that, in the near future, may prove to be the key that allows statistical physics to play a central role in the rapidly expanding field of molecular biology.

B. NMR Results

This is the actual situation regarding the lysozyme folding–unfolding process coming out from a large series of different experiments and in some way confirmed by MD simulations. However, the calorimetric experiments have detailed the unfolding process on considering that the energetic situation of the protein water system by means of proper heating–cooling cycles. On this frame recently has been considered new NMR studies made just on the behavior of the PCS, δ, of the water–lysozyme system ($h = 0.3$) in different thermal cycles covering the principal intervals, as proposed by the calorimetric experiment, of the process $N \rightleftarrows ID \longrightarrow D$.

We have conducted the several heating–cooling cycles: (A) the hydrated lysozyme was heated from 295 to 365K and than cooled up to 297K. In both the warming and the cooling, the PCS have been measured which steps of $\Delta T = 2$K, (B) the covered ranges was the following: heating from 296 to 366K and than the cooling up to 298K; thus in these A and B cycles all the $N \rightleftarrows ID \longrightarrow D$ process are explored. (C) In this cycle starting from 320K an interval from the N state to near after the T_{D}, that is, 347K, however, inside the $N \rightleftarrows ID$ region, was covered; (D) essentially the same T range of the cycle C is studied, but the cycle has been reversed by starting the cooling at 343K, just 3K before T_{D} (again inside the $N \rightleftarrows ID$ region); (E and F) are considered about the same T of the cycle D, starting from 320K we have reversed T at 341K, but at 330K we have stopped the thermal cycle. (G) The entire cycle was arranged inside the native N state.

The hydrated lysozyme ^{1}H NMR spectra measured in the cycle A upon the warming and cooling phases are shown in a three-dimensional plot in Fig. 26a and b, respectively. Figure 26a well displays the evolution from the native to the unfolded state; the intense peak (four orders of magnitude) centered at about 4.5 ppm belongs as it is well known to water and thus in our case to the hydration water protons whereas the others to protein protons. In the low-T regime these latter are almost completely smeared out meaning that protein side chains are not mobile on the NMR timescale at this hydration level. The situation change at about 325K, above this T, which is on the border between the native and the intermediate region, protein side chains increase their mobility. Furthermore, on increasing the T and in particular above 346K, clear and more resolved peaks appear in the spectrum. The reduction of the corresponding peak width is associated with an increased mobility. Figure 26b illustrating the spectral evolution during the cooling give evidence of the irreversibility showing that the protein side chains maintain a certain mobility also at the low, end cycle, temperatures.

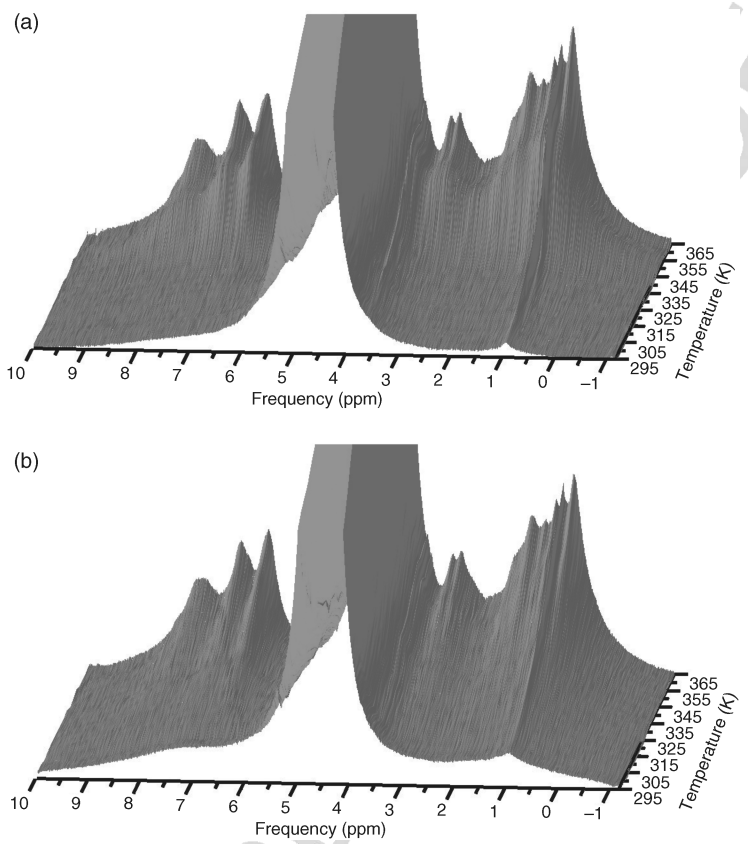

Figure 26. The ^{1}H NMR spectra (obtained from the FID, cycle A) of hydrated lysozyme (h = 0.3) upon the warming (**a**) and cooling (**b**) phases.

The Lorentzian form of the NMR spectral transfer function of the NMR instrument it is customarily used to analyze the measured spectra, in particular, the 4.5 ppm, water contribution . By performing such an analysis these behaviors are observed: in the case of the cycle G (the only one performed inside the native protein phase) only one Lorentzian form describes the spectra in both the warming and cooling phases, instead the final part of the heating phase of the cycle A and all its cooling parts are characterized by strong spectral changes. On these bases, such an approach furnishes a correct experimental procedure to test the level of reversibility in the protein folding process looking only to the hydration water. The absolute reversibility can be proved only when, within the experimental error,

the same Lorentzian (i.e., same parameters: chemical shift (δ), intensity, and HWHM $\Delta\nu$) fits the two ^{1}H NMR spectra measured respectively at the same T inside the different phases of a certain cycle.

Well different is, instead, the situation observed when the exploration was extended well inside the protein irreversible denaturation region. Two Lorentzians, appear just after the crossing of the border of the $ID \longrightarrow D$ phases, that is, where both the external protein hydration water and the internal one are detectable. When proteins unfold in an open polymeric structure, the internal water (also considering the effective high T) can easily break the HBs that link it to the protein residuals and can diffuse and interact with the external one. This reason explains the presence of two proton water NMR signals inside the phase D. One contribution for continuity is related with the protein hydration water whereas the second component with the internal water one. Both the components will survive in the measured spectra upto the end of the cooling phase. After the denaturation these two water forms are present in the system and can interact with each other or with the open biopolymer, in a complete different physical scenario if compared with the folded protein native state.

Figure 27 illustrates the thermal evolution of the measured ^{1}H NMR PCS, $\delta(T)$, for all the studied thermal cycles; are considered all data of the warming

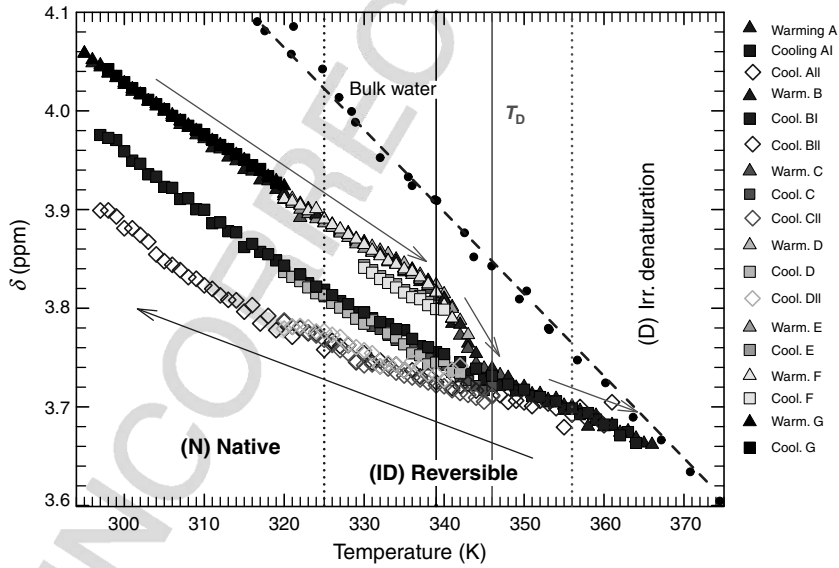

Figure 27. The evolution of the ^{1}H NMR chemical shift $\delta(T)$ in several thermal cycles of the lysozyme water. The pure bulk water chemical shift are also reported.

and cooling phases. For comparison are also reported the corresponding data of the pure bulk water. As it can be observed both the protein hydration water in the native phase and the bulk liquid chemical shifts $\delta(T)$ are characterized by a linear decreasing as T decreases. The protein hydration water behavior according to the previous considerations evolves differently in the warming and cooling phases, in addition whereas warming phase displays an identical T evolution of $\delta(T)$ for all the studied cycles, the cooling process is essentially characterized by the two main behaviors. As it can be observed in the high-T regime from 367 to about 350K, the PCS evolves, as a function of T, in same linear way of the warming phase with about the same values, whereas for $T < 350$K the situation is dominated by the behavior of the chemical shifts corresponding to the spectral contributions characterizing the system after than the irreversible folding have take place. A very interesting situation marks the warming phase, it is easy to observe a kink that starts at about 339K and stop near 350K. If we consider also the cycles E and F, the cooling process that starts few degrees above the onset of that kink, we observe that the corresponding PCS increases linearly by decreasing T but parallel to the data measured during the warming phase. This gives a sign that kink onset T could be considered as the end of the native state. In addition, a very important situation come out if we consider the analytical continuation of the measured protein hydration water $\delta(T)$ corresponding to the warming phase at highest temperatures (where essentially all water molecules are in the NHB-free state), we observe that such a quantity crosses the pure bulk water chemical shift at about 370K (i.e., just near the water boiling temperature).

In conclusion, we consider the use of these chemical shifts data to evaluate the configurational specific heat according to the procedure described above. Figure 28 shows $(-\partial \ln \delta(T)/\partial T)_P$ for lysozyme hydration evaluated from the reported $\delta(T)$ data for the different thermal cycles studied. In this figure are specifically reported the $(-\partial \ln \delta(T)/\partial T)_P$ data obtained for the warming part of the cycles A, B, C, D, E, and F; being the data of the different cooling phases practically identical the figure reports only the cycle A results. As it can be observed, the value of the observed maximum is within the experimental error the same measured by high-resolution calorimety [14]. There are some differences between the data of these latter experiments and the quantity obtained according to our procedure ($\sim C_{p,\mathrm{conf}}(T)$); one is represented by a nearly symmetric and narrow peak distribution than the one measured by means of the true calorimetry experiment (see, e.g., Fig. 2 and Ref. [14]). A second one is represented by the values characterizing the high-T region ($T > 350$), whereas in our data these values are almost the same as the ones measured in the opposite side of the peak; in the case of the calorimetric experiment, the C'_p values are higher in the high-T regime with respect to the opposite region. In addition, the C'_p measured in the cooling phase is represented by a large peaked distribution centered at about 335K. The reasons of these differences lie on the fact that the high-resolution calorimeters measure all the system contributions to the

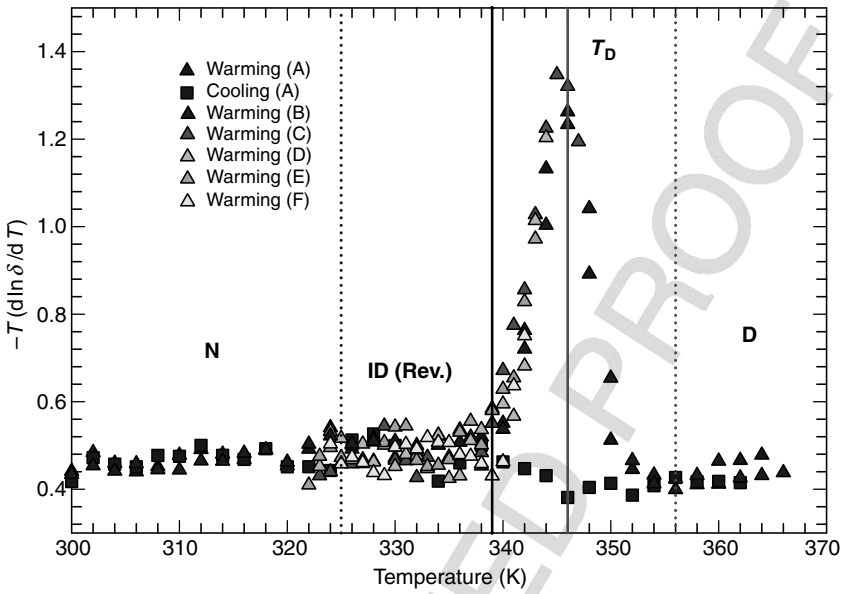

Figure 28. The configurational specific heat for all the cycles. It is worth noticing that the value of the obtained maximum is, within the experimental error, the same of that measured by high-resolution calorimeters.

specific heat, that is, vibrational and configurational, whereas we measure only a contribution proportional to the configurational energies associated with the protein folding. Another important and significant difference is that whereas in the true calorimetric experiments are macroscopically measured all the contributions to C'_p coming by all the system molecules (lysozyme and water), in our case we use only the water protons to probe locally the system configurational evolution as a function of T. The first macrosopic canonical approach is certainly more and more complete (all the energies corresponding to all the available degrees of freedom are evaluated) than the local one, but in a process in which the physics is essentially governed by configurational changes, like the protein folding, the latter one although furnishes only a quantity proportional to $C_{p,\mathrm{conf}}(T)$ appears to be more useful than the other ones. Therefore, the quantity reported in Fig. 28 represents the lysozyme folding process evaluated in terms of the macromolecule configurational changes. In addition to the calorimetric data, we find that the temperature of 339K, as intuitively deducted being the temperature of the chemical shift kink (and also of the configurational entropy), represents the start point of the calorimetric peak.

V. CONCLUSIVE NOTES

We have surveyed a wide range of research on proteins hydration water. Of paramount importance are the two observed crossover, which, on the basis of the many results we have described, can be considered responsible for the biological activity of macromolecules, including RNA and DNA. Neutron measurements of the MSD indicate, surprisingly, that the crossover temperature of biopolymer and its hydration water are closely synchronized. More precisely, FTIR experiments indicate that when a biosystem restores its dynamics, the solvent crosses from a strong to a fragile liquid, that is, the HB networking changes from a thermal state in which LDL dominates to one in which HDL dominates. At the same time, irreversible denaturation takes place when the HB numbers decrease to values for which only a few water molecules are bonded.

Finally, we have comparatively considered our obtained configurational specific heat with the one observed in the high-resolution calorimetric experiments[14]. Although the results on the $C_p(T)$ characterized by a marked maximum at about the same temperature T_{D} ($\sim$ 346K) are similar, we have confirmation that all the unfolding process is due exclusively to changes in the system configurational degrees of freedom.

More precisely, by exploring the water–lysozyme system in proper thermal cycles, indicate that the protein denaturation takes place by considering the macromolecule in terms of a three-stage model: a native structure (compact and globular) that evolves in an intermediate state (globular, open, or molten) through a reversible transition and finally in the irreversible denatured state as an essentially unfolded polymer chain (a sort of disordered coil). Thus, a progressive conformational change occurs from the native globular structure to that of an open coil in which the protein interactions are switched off, and the macromolecular packing decreases at each of the steps characterizing the entire $N \rightleftarrows ID \longrightarrow D$ process. In all the three states, it is determinant the role of the protein water (the hydration and the internal).

ACKNOWLEDGMENTS

Research in Messina is supported by the PRA-Unime- 2005 and PRIN2008. Research at Massachusetts Institute of Technology is supported by Department of Energy Grants DE-FG02-90ER45429 and 2113- MIT-DOE-591. Research at Boston University is supported by National Science Foundation Chemistry Division Grants CHE0616489, CHE0908218, and CHE0911389. This work utilized facilities supported in part by the National Science Foundation under Agreement DMR-0086210. We acknowledge the corresponding publishers for the permissions to reproduce figures 1, 6–9, 11, 17–19.

REFERENCES

1. P. Ball, *Chem. Rev.* **108**, 74–108 (2008).
2. J. A. Rupley and G. Careri, *Adv. Protein Chem.* **41**, 37 (1991).
3. J. A. Rupley, P. H. Yang, and G. Tollin, *Water in Polymers*, Vol. 127. S. P. Rowland, ed., ACS Symposium Series, 1980, p. 111.
4. R. B. Gregory, *Protein Solvent Interaction*, Marcel Dekker, New York, 1995.
5. C. A. Angell, M. Oguni, and W. J. Sichina, *J. Phys. Chem.* **86**, 998 (1982).
6. P. G. Debenedetti and H. E. Stanley, *Phys. Today* **56**, 40 (2003).
7. O. Mishima and H. E. Stanley, *Nature* **396**, 329 (1998).
8. I. R. T. Iben, et al., *Phys. Rev. Lett.* **62**, 1916–1919 (1989).
9. C. A. Angell, *Science* **319**, 582 (2008).
10. F. Parak and E. W. Knapp, *Proc. Natl. Acad. Sci. USA* **81**, 7088–7092 (1984).
11. W. Doster, S. Cusak, and W. Petry, *Nature* **337**, 754–756 (1989).
12. B. F. Rasmussen, M. Stock, D. Ringe, and G. A. Petsko, *Nature* **357**, 423–424, (1992).
13. G. Caliskan, A. Kisliuk, and A. P. Sokolov, *J. Non-Cryst. Sol.* **868**, 307–310 (2002).
14. G. Salvetti, E. Tombari, L. Mikheeva, and G. P. Johari, *J. Phys. Chem. B.* **106**, 6081–6087 (2002).
15. F. Mallamace, et al., *Proc. Natl. Acad. Sci. USA* **105**, 12725 (2008).
16. H. E. Stanley, et al., *Physica A* **386**, (2007).
17. S.-H. Chen, et al., *Proc. Natl. Acad. Sci. USA* **103**, 9012 (2006).
18. F. Mallamace, et al., *Proc. Natl. Acad. Sci. USA* **104**, 424 (2007).
19. F. Mallamace, et al., *J. Chem. Phys.* **127**, 045104 (2007).
20. S.-H. Chen, et al., *J. Chem. Phys.*, **125**, 171103, (2006).
21. L. Liu, A. Faraone, and S.-H. Chen, *Phys. Rev. E* **65**, 041506 (2002).
22. S. H. Chen and M. Kotlarchyk, *Interaction of Photons and Neutrons with Matter*, 2nd ed., World Scientific Publishing Co. Pre., 2007.
23. G. Zaccai, *Science* **288**, 1604 (2000).
24. M. Bee, *Quasielastic Neutron Scattering*, Adam Hilger, Philadelphia, 1988.
25. W. Goetze and L. Sjoegren, *Rep. Prog. Phys.* **55**, 241 (1992).
26. X. Q. Chu, E. Fratini, P. Baglioni, A. Faraone, and S. H. Chen, *Phys. Rev. E* **77**, 011908 (2008).
27. K. Heremans and L. Smeller, *Biochim. Biophys. Acta* **1386**, 353–370 (1998).
28. M. I. Marques, J. M. Borreguero, H. E. Stanley, and N. V. Dokholyan ,*Phys. Rev. Lett.* **91**, 138103 (2003).
29. X. Q. Chu, et al., *J. Phys. Chem. B*, **113**, 5001 (2009).
30. Y. Zhang, et al., *J. Phys.: Condens. Matter* 2008, **20**, 502101 (2008).
31. X. Q. Chu, A. I. Kolesnikov, A. P. Moravsky, V. Garcia-Sakai, and S. H. Chen, *Phys. Rev E* **76** 021505–021510 (2007).
32. B. B. Boonyaratanakornkit, C. B. Park, and D. S. Clark Biochim. *Biophys. Acta* **1595**, 235–249 (2002).
33. P. Kolakowski, E. Dumay, and J. C. Cheftel, *Food Hydrocolloids* **15**, 215–232 (2001).
34. Y.-J. Jung, J. P. Garrahan, and D. Chandler, *Phys. Rev. E* **69**, 061205 (2004).
35. A. P. Sokolov, H. Grimm, A. Kisliuk, and A. J. Dianoux, *J. Chem. Phys.* **110**, 7053 (1999).

36. M. Tarek and D. J. Tobias, *Phys. Rev. Lett.* **88**, 138101 (2002).
37. H. Hartmann, et al., *Proc. Natl. Acad. Sci. USA* **79**, 4067 (1982).
38. A. L. Tournier, J. Xu, and J. C. Smith, *Biophys. J.* **85**, 1871 (2003).
39. A. L. Lee and A. J. Wand, *Nature* **411**, 501 (2001).
40. P. Kumar, et al., *Phys. Rev. Lett.* **97**, 177802 (2006).
41. E. Lindahl, B. Hess, and D. van der Spoel, *J. Mol. Modeling* **7**, 306 (2001).
42. P. J. Artymiuk, C. C. F. Blake, D. W. Rice, and K. S. Wilson, *Acta Crystallogr.* **B 38**, 778 (1982).
43. H. R. Drew, et al., *Proc. Natl. Acad. Sci. USA* **78**, 2179 (1981).
44. Z. Yan, S. V. Buldyrev, N. Giovambattista, P. G. Debenedetti, and H. E. Stanley, *Phys. Rev. E* **73**, 051204 (2006).
45. M. Tarek and D. J. Tobias *Phys. Rev. Lett.* **88**, 138101 (2002).
46. J. Swenson, *Phys Rev. Lett.* **97**, 189801 (2006); J. Swenson, H. Jansson, J. Hedstrom, and R. Bergman, *J. Phys.: Condens. Matter* **19**, 205109 (2007).
47. S.-H. Chen, L. Liu, and A. Faraone, *Phys Rev. Lett*. **97**, 189803 (2006).
48. W. L. Jorgensen and J. J. Tirado-Rives, *Am. Chem. Soc*. **110**, 1657–1666 (1988).
49. M. Tarek and D. J. Tobias, *Biophys. J.* **79**, 3244–3257 (2000).
50. M. Tarek and D. J. Tobias *Phys. Rev. Lett.* **89**, 275501 (2002).
51. M. Lagi, X. Q. Chu, C. S. Kim, Mallamace, F., Baglioni, and P. S. H. Chen, *J. Phys. Chem. B* **112**, 1571–1575 (2008).
52. F. Merzel and J. C. Smith, *Proc. Natl. Acad. Sci. USA* **99**, 5378–5383 (2002).
53. J. Swenson, H. Jansson, and R. Bergman, *Phys. Rev. Lett.* **96**, 247802 (2006).
54. A. Huwe, et al., *J. Phys. IV (France)*, **10**, 59 (2000).
55. D. Bertolini, M. Cassettari, and P. Savetti, *J. Chem. Phys.* **76**, 3285 (1982).
56. R. Torre, P. Bartolini, and R. Righini, *Nature* **428**, 296 (2004).
57. F. Mallamace, J. C. Earnshaw, N. Micali, S. Trusso, and C. Vasi, *Physica A* **231**, 207 (1996).
58. C. Rønne, P-O. Åstarnd, and S. R. Keiding, *Phys. Rev. Lett.* **82**, 2888 (1999).
59. J. Swenson, R. Bergman, and S. Longeville, *J. Chem. Phys.* **115**, 11299 (2001).
60. H. Jansson and J. Swenson, *Eur. Phys. J. E* **12**, S51 (2003).
61. J. Swenson, H. Jansson, W. S. Howells, and S. Longeville, *J. Chem. Phys.* **122**, 084505 (2005).
62. L. Liu, S.-H. Chen, A. Faraone, C.-W. Yen, and C.-Y. Mou, *Phys. Rev. Lett.* **95**, 117802 (2005).
63. K. Yoshida, T. Yamaguchi, S. Kittara, M. C. Bellissent-Funel, and P. Fourquet, *J. Chem. Phys.* **129**, 054702 (2008).
64. P. Gallo, M. Rovere, and S.-H. Chen, *J. Phys. Chem. Lett.* **1**, 729 (2010).
65. M. Paolantoni, P. Sassi, A. Morresi, and S. Santini, *J. Chem. Phys.* **127**, 024504 (2007).
66. D. W. Hwang, C.-C. Chu, A. K. Sinha, and L.-P. Hwang, *J. Chem. Phys.* **127**, 044702 (2007).
67. S.H. Chen, J. Teixeira, and R. Nicklow, *Phys. Rev.* **26**, 3477 (1982).
68. J. Teixeira, A. Luzar, and S. Longeville, *J. Phys.: Condens. Matter* **18**, S2353 (2006).
69. R. Bergman, J. Mattson, C. Svanberg, G. A. Schwartz, and J. Swenson, *Europhys. Lett.* **64**, 675 (2003).
70. J. Swenson, G. A. Schwartz, R. Bergman, and W. S. Howells, *Eur. Phys. J. E* **12**, 179 (2003).
71. W. Doster and M. Settles, *Biochim. Biophys. Acta* **1749**, 173 (2005).
72. H. Jansson and J. Swenson, *Biochim. Biophys. Acta* **1804**, 20 (2010).

73. W. Doster, et al., *Phys. Rev. Lett.* **104**, 098101 (2010).
74. Y. Zhang, et al., *J. Chem. Phys.* **130**, 135101 (2009).
75. A. Hedoux, et al., *J. Chem Phys.* **124**, 014703 (2006).
76. L. Smeller, F. Meersman, and K. Heremans, *Biochim. Biophys. Acta* **1764**, 497 (2006).
77. A. Scala, F. Starr, E. La Nave, F. Sciortino, and H. E. Stanley, *Nature* **406**, 166 (2000).
78. C. A. Angell, E. D. Finch, L. A. Woolf, and P. Bach, *J. Chem. Phys.* **65**, 3063–3066 (1976).
79. S. J. Suresh and V. M. Naik, *J. Chem. Phys.* **113**, 9727 (2000).
80. K. Wood, et al., *J. Am. Chem. Soc.* **130**, 4586 (2008).
81. G. Sposito, *J. Chem. Phys.* **74**, 6943–6949 (1981).
82. S.-H. Chen, et al., *Proc. Natl. Acad. Sci. USA* **103**, 12974 (2006).
83. M. G. Mazza, N. Giovambattista, H. E. Stanley, and F. W. Starr, *Phys. Rev. E* **76**, 031202 (2007).
84. F. Mallamace, et al., *Proc. Natl. Acad. Sci. USA* **104**, 18387 (2007).